Single-Snapshot Angle and Incremental Range Estimation for FDA-MIMO Radar

Lan Lan, *Member, IEEE*, Massimo Rosamilia *Student Member, IEEE*, Augusto Aubry, *Senior Member, IEEE*, Antonio De Maio, *Fellow, IEEE*, Guisheng Liao, *Senior Member, IEEE*

***Abstract*—This paper deals with the problem of angle and incremental range (i.e., the target range offset with respect to the center of the cell under test) estimation with a frequency diverse-array multiple-input multiple-output (FDA-MIMO) radar exploiting as observable a single data snapshot. Starting from the observation that the maximum likelihood (ML) estimation entails a two-dimensional grid search over the parameters of interest, three approximated ML techniques are designed resorting to the coordinate descent algorithm and the adaptive monopulse criterion (employing either real or complex slope/bias corrections). At the analysis stage, the estimation performance of the proposed methods, including the tapered and double-step monopulse versions, is assessed also in comparison with the Cramer-Rao lower Bound (CRB). Numerical results corroborate the effectiveness of the considered estimation strategies in some diverse simulated scenarios.**

***Index Terms*—FDA-MIMO radar, target parameters estimation, monopulse, coordinate descent, bias correction.**

I. Introduction

Estimation of target parameters is an enduring signal processing problem that has always raised persistent attention within the radar scientific community. The emergence of new threats call for stressing and stressing radar performance requirements as well as the development of advanced algorithms capable of providing reliable estimates of the target position, even at the expense of an increased computational complexity. With reference to the direction-of-arrival (DOA), it is known that the phased-array radar can achieve highly accurate angle estimation by precisely forming a beam in the desired direction [1, 2]. In particular, the problem of angle estimation is typically solved resorting to the Maximum Likelihood (ML) technique, which has the advantage of being asymptotically unbiased and efficient at the expense of an high computational complexity associated with the required multidimensional search. To this end, a fair amount of alternative methodologies have been developed, such as the adaptive monopulse criterion [3], the generalized adaptive multidimensional monopulse algorithm based on a series expansion of the array manifold [4], and combined constrained methods [5, 6]. Nevertheless, it is worth pointing out that in a classic phased array radar system the beampattern is dependent only on the angular direction [7–10] but it is not selective in the range domain. As a consequence, the range information is not directly embedded in the beamforming process. To overcome this drawback, a novel beam scanning array, referred to as frequency diverse array (FDA), has been proposed [11–13]. Specifically, employing a small frequency increment across adjacent array elements, the FDA induces discrimination in both the angle and range domain. Once adequately exploited, it can allow to glean jointly range and angle information. Besides, the mentioned extra flexibility of the FDA radar paves the way for its capitalization in several applications, such as cognitive target tracking [14] and target localization [15]. Furthermore, FDA can be successfully twisted with a multiple-input multiple-output (MIMO) architecture leading to a FDA-MIMO radar [16], where additional degrees-of-freedom (DOFs) are available by separating the different transmitted waveforms with appropriate matched filtering. Therefore, a range-angle-dependent transreceive beampattern is realized via the FDA-MIMO manifold structure. In this context, a variety of applications have been proposed in the open literature, such as the suppression of deceptive main-lobe jammers (from the same azimuth, but different range, as the target of interest) [17], range ambiguous clutter suppression with airborne radar [18], and synthetic aperture radar (SAR) imaging with improved resolution [19]. Not surprisingly, a substantial bulk of work has been focused on the target parameters estimation, via rotational invariant techniques (ESPRIT) [20], multiple signal classification (MUSIC) [21] and/or combined MUSIC-ESPRIT methods [22], compressed sensing-based algorithms [23], and sparse reconstruction [24].

Capitalizing the additional DOFs of FDA-MIMO radar in the range domain, the target angle and range can be simultaneously estimated due to the range-angle-dependent characteristic of the FDA-MIMO steering vector. Several system configurations, e.g., the bistatic FDA-MIMO [25], the transmit subarray FDA-MIMO (TS-FDA) [26], and the unfolded co-prime FDA-MIMO [27] have been studied for the mentioned purpose. However, in some practical applications with high pulse repetition frequency (PRF), the range ambiguity problem may be encountered, leading to a degradation of the estimation accuracy. To overcome this shortcoming, employing a specific design of the frequency increment, in [28] the authors have developed a range ambiguity resolving technique to estimate the index of the ambiguity interval. As a drawback, a large number of snapshots are required. Finally, in [28], the Cramér-

This work of Lan Lan was supported in part by the National Nature Science Foundation of China under Grants 61931016 and 62071344.

M. Rosamilia, A. Aubry and A. De Maio are with the Department of Electrical Engineering and Information Technology, University of Naples "Federico II", I-80125 Naples, Italy. (e-mail: massimo.rosamilia@unina.it; augusto.aubry@unina.it; ademaio@unina.it). (Corresponding author: Antonio De Maio.)

Lan Lan and Guisheng Liao are with the National Key Laboratory of Radar Signal Processing, Xidian University, Xi'an 710071, China, (e-mail: lanlan@xidian.edu.cn; liaogs@xidian.edu.cn);

Rao lower Bound (CRB), for range and angle estimation via a FDA-MIMO radar is computed assuming the presence of structured interference plus background noise.

Despite its key role in many practical high-precision applications, the estimation of the incremental range (target displacement with respect to (w.r.t.) the center of the occupied range cell) has only received a limited attention. This observation motivates the study of this paper which investigates the problem of joint target angle and incremental range estimation using a FDA-MIMO radar in a background of Gaussian interference with known spectral properties. At the design stage, the target parameters, i.e., angle, incremental range, and echo-amplitude, are assumed unknown. Under the aforementioned setup, the estimation problem is formulated starting from a single data snapshot. Then the ML estimator is derived maximizing the likelihood function w.r.t. the unknown parameters. Furthermore, to reduce the computational cost connected with the two-dimensional (2-D) grid search required by the implementation of ML rule, three approximated methods are considered:

- an iterative procedure based on the coordinate descent (CD) algorithm leveraging a sequence of one-dimensional (1-D) searches which arise alternating between the optimization over one variable keeping the other fixed;
- an adaptive monopulse approach which approximates the optimal search exploiting real bias/slope correction values;
- a generalized monopulse procedure employing a complex slope and bias correction aimed at minimizing the mean square value of the noise error term.

At the analysis stage, CRBs for the angle and incremental range estimation via a FDA-MIMO radar are derived. The root mean square errors (RMSEs) of the estimates versus the input signal-to-interference-plus-noise ratio (SINR) are provided. Besides, an extensive bias and variance analysis is developed to show the the effectiveness of the considered approximated estimation methods (including tapered and double-step versions of the monopulse procedures).

The paper is organized as follows. Section II presents the signal model for FDA-MIMO radar. In Section III, the single snapshot angle and incremental range estimation problem is formulated. Besides, the ML estimator and the three aforementioned approximated methods are introduced. The CRBs for angle and incremental range are computed in Section IV, whereas performance analysis is addressed in Section V. Finally, conclusions and possible future research developments are discussed in Section VI.

Notations: Boldface is used for vectors $\boldsymbol{x}$ (lower case) whose n-th entry is $x(n)$, and matrices $\boldsymbol{A}$ (upper case) whose (m,n)-th entry is $A_{m,n}$. A matrix $\boldsymbol{A} \in \mathbb{C}^{N\times M}$ can also be defined by its columns $\boldsymbol{a}_m \in \mathbb{C}^N,\ m = 1,\ldots,M$ (i.e., $\boldsymbol{A} = [\boldsymbol{a}_1,\ldots,\boldsymbol{a}_M]$). The transpose, the conjugate, and the conjugate transpose operators are denoted by the symbols $(\cdot)^{\mathrm{T}}$, $(\cdot)^*$, and $(\cdot)^\dagger$, respectively. $\mathrm{diag}(\boldsymbol{x})$ indicates the diagonal matrix whose i-th diagonal element is the i-th entry of $\boldsymbol{x}$. $\boldsymbol{I}$, $\boldsymbol{0}$ and $\boldsymbol{1}$ denote respectively the identity matrix, the matrix with zero entries and the vector with all elements being one (their size is determined from the context). $\mathbb{R}^N$, $\mathbb{C}^N$, $\mathbb{C}^{N\times M}$, and $\mathbb{H}^N$ are respectively the sets of N-dimensional vectors of complex numbers, N-dimensional vectors real numbers, $N\times M$ complex matrices, and $N\times N$ Hermitian matrices. The determinant of the matrix $\boldsymbol{A}\in\mathbb{C}^{N\times N}$ is indicated with $\det(\boldsymbol{A})$. For any $\boldsymbol{x}\in\mathbb{C}^N$, $\|\boldsymbol{x}\|$ denotes its Euclidian norm. $\odot$ and $\otimes$ represent the Hadamard (element-wise) product and the Kronecker product, respectively. The letter j represents the imaginary unit (i.e. $j=\sqrt{-1}$). For any complex number z, $\Re(z)$, $\Im(z)$, and $|z|$ are used to denote the real part, imaginary part, and the modulus of z, respectively. $[a,b]$ indicates a closed interval of $\mathbb{R}$. Finally, $\mathbb{E}[\cdot]$ denotes the statistical expectation.

II. Signal Model of FDA-MIMO Radar

A. Transmitted Signal Model

Let us consider a colocated FDA-MIMO radar consisting of M transmit and N receive modules placed according to a uniform linear array configuration in both transmission and reception (see Fig. 1) [29]. A frequency increment Δf is introduced element-by-element in the transmit array with the first array-element being the reference. Thus, the carrier frequency at the m-th Tx element is

$$f_m = f_0 + (m-1)\Delta f, \quad m = 1,2,\cdots,M, \tag{1}$$

where f_0 indicates the reference carrier. Each element transmits a specific base-band phase-modulated pulse, which is composed of P subpulses, and the resulting complex envelope of the Radio Frequency (RF) signal radiated by the m-th element can be expressed as

$$s_m(t) = \sqrt{\frac{E}{P}} x_m(t) e^{j2\pi f_m t}, \quad 0\le t\le T_p, \tag{2}$$

where E is the transmitted energy, T_p is the radar pulse duration, and

$$x_m(t) = \frac{1}{\sqrt{\tau_b}} \sum_{p=1}^{P} \varphi_m(l)\, u\left[\frac{t-(p-1)\tau_b}{\tau_b}\right], \quad p = 1, \ \cdots, P, \tag{3}$$

$\tau_b = \frac{T_p}{P}$, $u(t)$ is the asymmetric rect function, i.e., $u(t)=1$ as long as $0\le t\le 1$ and zero elsewhere, and $\varphi_m(p) = e^{j\phi_m(p)}$, with $\phi_m(p)\in[0,2\pi]$.

B. Received Signal Model

For a point-like target with a constant radar cross-section (RCS) over the FDA-MIMO radar bandwidth, located in far-field at the angle θ_t and range R_t (see Fig. 1) [30, 31], the complex envelope of the signal received by the n-th radiating element ($n = 1,2,\cdots,N$) due to the signal transmitted by the m-th antenna ($m = 1,2,\cdots,M$) can be expressed as [29]

$$\begin{aligned} y_{m,n}(t) &= \beta x_m(t-\tau_{m,n}) e^{j2\pi f_m(t-\tau_{m,n})} \\ &\approx \beta x_m(t-\tau_0) e^{j2\pi f_m(t-\tau_{m,n})}, \end{aligned} \tag{4}$$

where $\tau_{m,n} = \frac{2R_t - d(n-1)\sin(\theta_t) - d(m-1)\sin(\theta_t)}{c}$ is the round-trip propagation time, β is the complex echo amplitude (accounting for the transmit amplitude, phase, target reflectivity,

This article has been accepted for publication in IEEE Transactions on Aerospace and Electronic Systems. This is the author's version which has not been fully edited and content may change prior to final publication. Citation information: DOI 10.1109/TAES.2021.3083591

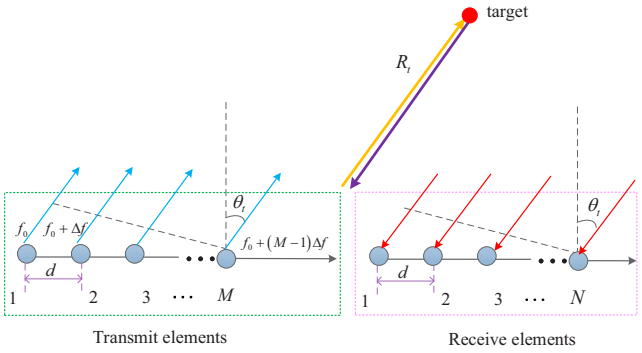

Fig. 1: Signal transmission and reception in FDA-MIMO radar.

and channels propagation effects), d is the array's inter-element spacing, and c is the speed of light. The approximation relies on the narrowband assumption, i.e., $x_m(t-\tau_{m,n}) \approx x_m(t-\tau_0)$, with $\tau_0 = \frac{2R_t}{c}$ the customary envelope time delay.

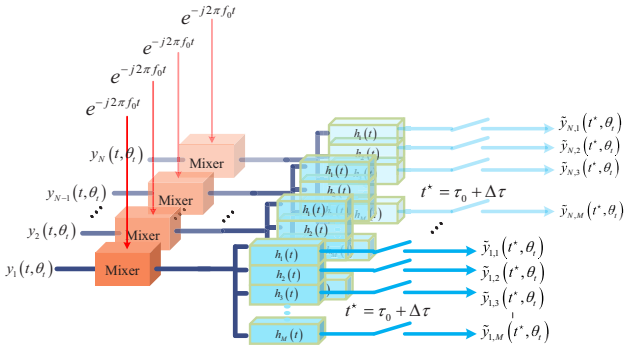

Fig. 2: Signal processing at the receiver with multiple match-filtered waveforms.

After the pre-processing of Fig. 2, it can be shown that, under some mild technical conditions (see Appendix A of [29]), the received useful samples from the CUT can be stacked to form a $MN \times 1$-dimensional vector

$$\begin{aligned} \boldsymbol{y}_{\mathrm{S}} &= \beta_1 \boldsymbol{b}(\theta_t) \otimes [\boldsymbol{c}(\theta_t) \odot \boldsymbol{a}(\Delta\tau)] \\ &= \beta_1 \boldsymbol{s}(\theta_t, \Delta\tau), \end{aligned} \tag{5}$$

where $\boldsymbol{s}(\theta_t,\Delta\tau) = \boldsymbol{b}(\theta_t) \otimes [\boldsymbol{c}(\theta_t) \odot \boldsymbol{a}(\Delta\tau)] \in \mathbb{C}^{MN}$ with $\Delta\tau$ the incremental delay w.r.t. the sampling time associated with the target range cell [29], $\boldsymbol{b}(\theta_t) = \left[1, e^{j2\pi\frac{d}{\lambda_0}\sin(\theta_t)}, \cdots, e^{j2\pi\frac{d}{\lambda_0}(N-1)\sin(\theta_t)}\right]^{\mathrm{T}} \in \mathbb{C}^N$ denotes the angle-dependent receive steering vector, $\boldsymbol{c}(\theta_t) = \boldsymbol{R}^{\mathrm{T}}\boldsymbol{d}(\theta_t) \in \mathbb{C}^M$ with $\boldsymbol{d}(\theta_t) = \left[1, e^{j2\pi\frac{d}{\lambda_0}\sin(\theta_t)}, \cdots, e^{j2\pi\frac{d}{\lambda_0}(M-1)\sin(\theta_t)}\right]^{\mathrm{T}} \in \mathbb{C}^M$ the angle-dependent transmit steering vector and $\boldsymbol{R} \in \mathbb{C}^{M\times M}$ the transmit waveforms correlation matrix, i.e., $R_{m,l} = \int_0^{T_p} x_m(s)\, x_l^*(s) ds$, $(m,n) \in \{1,...,M\}^2$, and $\boldsymbol{a}(\Delta\tau) = \left[1, e^{j2\pi\Delta f\Delta\tau} \cdots, e^{j2\pi\Delta f(M-1)\Delta\tau}\right]^{\mathrm{T}} \in \mathbb{C}^M$ indicates the range-dependent steering vector.

III. Joint Angle-Range Estimation for FDA-MIMO Radar

This section investigates parameters estimation in FDA-MIMO radar. Let us assume the availability of a single data snapshot $\boldsymbol{z} \in \mathbb{C}^{MN}$ containing the superposition of the useful target signal and interference plus noise contribution [3, 32], namely the vector of observables can be cast as

$$\boldsymbol{z} = \beta_1 \boldsymbol{s}(\theta_t, \Delta\tau) + \boldsymbol{n}, \tag{6}$$

where $\boldsymbol{n} \in \mathbb{C}^{MN}$ is modeled as zero-mean complex circularly symmetric Gaussian random vector, i.e., $\boldsymbol{n} \sim \mathcal{CN}(0, \boldsymbol{Q})$ with $\boldsymbol{Q} \in \mathbb{H}^{MN}$ the positive definite covariance matrix of the interference plus noise term. Therein, θ_t and $\Delta\tau$ describe the unknown angle and incremental range to be estimated, respectively. Now, letting $u = \sin(\theta_t)$ (complying with $|u| \le 1$) and $\delta = 2\Delta f \Delta\tau$ (satisfying $|\delta| \le \frac{\Delta f}{B}$), $\boldsymbol{s}(\theta_t, \Delta\tau)$ can be further expressed as

$$\begin{aligned} \boldsymbol{s}(\theta_t, \Delta\tau) &= \boldsymbol{s}(u, \delta) \\ &= \boldsymbol{b}(u) \otimes [\boldsymbol{c}(u) \odot \boldsymbol{a}(\delta)], \end{aligned} \tag{7}$$

where $\boldsymbol{b}(u) = \left[1, e^{j2\pi\frac{d}{\lambda_0}u}, \cdots, e^{j2\pi\frac{d}{\lambda_0}(N-1)u}\right]^{\mathrm{T}} \in \mathbb{C}^N$, $\boldsymbol{c}(u) = \boldsymbol{R}^{\mathrm{T}}\boldsymbol{d}(u) \in \mathbb{C}^M$ with $\boldsymbol{d}(u) = \left[1, e^{j2\pi\frac{d}{\lambda_0}u}, \cdots, e^{j2\pi\frac{d}{\lambda_0}(M-1)u}\right]^{\mathrm{T}} \in \mathbb{C}^M$, and $\boldsymbol{a}(\delta) = \left[1, e^{j\pi\delta} \cdots, e^{j\pi(M-1)\delta}\right]^{\mathrm{T}} \in \mathbb{C}^M$.

In the following subsections, the ML Estimator (MLE) of u and δ is introduced and three low complexity methods are proposed to approximate the MLE computation.

A. ML Estimation of u and δ

In this subsection, the ML estimation problem is formalized as the constrained maximization (w.r.t. the unknown parameters, i.e., β_1, u and δ [32]) of the likelihood function,

$$f(u,\delta,\beta_1;\boldsymbol{z}) = \frac{1}{\pi^{MN}\det(\boldsymbol{Q})} e^{-\left[(\boldsymbol{z}-\beta_1\boldsymbol{s}(u,\delta))^\dagger \boldsymbol{Q}^{-1}(\boldsymbol{z}-\beta_1\boldsymbol{s}(u,\delta))\right]}. \tag{8}$$

This is equivalent to minimizing the following quadratic form

$$\min_{\substack{\beta_1\in\mathbb{C}, u\in[-1,1],\\ \delta\in[-\frac{\Delta f}{B},\frac{\Delta f}{B}]}} (\boldsymbol{z}-\beta_1\boldsymbol{s}(u,\delta))^\dagger \boldsymbol{Q}^{-1}(\boldsymbol{z}-\beta_1\boldsymbol{s}(u,\delta)). \tag{9}$$

Now, concentrating (9) over β_1 yields

$$\hat{\beta}_1 = \frac{\boldsymbol{s}^\dagger(u,\delta)\boldsymbol{Q}^{-1}\boldsymbol{z}}{\boldsymbol{s}^\dagger(u,\delta)\boldsymbol{Q}^{-1}\boldsymbol{s}(u,\delta)}. \tag{10}$$

Hence, substituting (10) into the objective function of (9) as well as dropping constant and irrelevant terms leads to

$$\max_{u\in[-1,1],\delta\in[-\frac{\Delta f}{B},\frac{\Delta f}{B}]} \frac{\left|\boldsymbol{s}^\dagger(u,\delta)\boldsymbol{Q}^{-1}\boldsymbol{z}\right|^2}{\boldsymbol{s}^\dagger(u,\delta)\boldsymbol{Q}^{-1}\boldsymbol{s}(u,\delta)}. \tag{11}$$

Finally, the ML estimates of u and δ can be obtained as maximizers of

$$P(u,\delta) = |\boldsymbol{w}_0{}^\dagger(u,\delta)\boldsymbol{z}|^2, \tag{12}$$

where $\boldsymbol{w}_0(u,\delta) = \left[\boldsymbol{s}^\dagger(u,\delta)\boldsymbol{Q}^{-1}\boldsymbol{s}(u,\delta)\right]^{-\frac{1}{2}}\boldsymbol{Q}^{-1}\boldsymbol{s}(u,\delta) \in \mathbb{C}^{MN}$.

B. Approximated Methods for Range and Angle Estimation

The ML rule can be practically implemented via a 2-D grid search. To reduce the computational cost required by the foregoing procedure, it is valuable to design approximated solution methods. To this end, this section is focused on designing: 1) a CD algorithm; 2) adaptive monopulse procedures (AMP).

1) Coordinate Descent Algorithm

An approximation of the optimal 2-D search involved in (12) is developed via the CD method. This leads to a sequence of one-dimensional (1-D) searches obtained alternating between the optimization over each variable keeping the other fixed. The problem of finding the maximizer of each 1-D search is tackled using the grid search method where the feasible interval of interest is discretized in a finite set of points. Specifically, the 1-D searches w.r.t. u and δ are respectively conducted over the discretized intervals $\mathcal{I}_u$ and $\mathcal{I}_\delta$, defined as

$$\mathcal{I}_u = \{-1 + \frac{2i}{N_u},\ i = 0,\ldots,N_u\} \tag{13a}$$

and

$$\mathcal{I}_\delta = \{-\frac{\Delta f}{B} + \frac{2i}{N_\delta}\frac{\Delta f}{B},\ i = 0,\ldots,N_\delta\}, \tag{13b}$$

where (N_u+1) and $(N_\delta+1)$ are the number of discrete points considered for the optimization over u and δ, respectively. It is also worth pointing out that it is not possible to establish *a-priori* which order of optimization leads to the best estimate, i.e., first optimize u and then optimize δ, or vice versa. To overcome this problem, the CD-based algorithm considered herein is applied twice, one for each possible initial search direction. Therefore, among the two obtained solutions, the one that maximizes (12) is chosen as estimate. The exit condition (for each updating policy) is set as $D^n \leq \varepsilon$ with $\varepsilon > 0$ and $D^n = |P^n - P^{n-1}|$, where

$$P^n = |(\boldsymbol{w}^n)^\dagger \boldsymbol{z}|^2 \tag{14}$$

indicates the objective function at the n-th iteration with

$$\boldsymbol{w}^n = \left[\boldsymbol{s}^\dagger\left(\hat{u}^n,\hat{\delta}^n\right)\boldsymbol{Q}^{-1}\boldsymbol{s}\left(\hat{u}^n,\hat{\delta}^n\right)\right]^{-\frac{1}{2}}\boldsymbol{Q}^{-1}\boldsymbol{s}\left(\hat{u}^n,\hat{\delta}^n\right). \tag{15}$$

Letting u_0 and δ_0 the nominal angle and range, the initial estimates are chosen as $\hat{u}^0 = u_0$ and $\hat{\delta}^0 = \delta_0$. The resulting method is summarized in **Algorithm 1**.

Note that in the presence of two blocks/variables, regardless of the initial search direction, the CD approach (starting from the second iteration) coincides with the Maximum Block Improvement (MBI) policy [33]. Therefore, invoking the convergence properties of MBI [33–35], any limit point resulting from **Algorithm 1** is a stationary point to Problem (12), although convergence to the optimal value cannot be claimed [36].

Leveraging the output of **Algorithm 1** the estimates of u and δ obtained via the CD method are given by

$$u_{\mathrm{CD}} = \hat{u} \tag{16}$$

Algorithm 1 FDA-CD

Input: u_0, δ_0, $\boldsymbol{z}$, $\boldsymbol{Q}$, $\boldsymbol{s}$, ε
Output: A solution $\hat{u}$, $\hat{\delta}$ to (11).
Initialization: $n = 0$, $\hat{u}^0 = u_0$, $\hat{\delta}^0 = \delta_0$, $P^0 = P(\hat{u}^0,\hat{\delta}^0)$
repeat (optimization for initial search direction given by u)
1. Find $\hat{u}^{n+1} = \arg\max_{u\in\mathcal{I}_u} P(u,\hat{\delta}^n)$;
2. Find $\hat{\delta}^{n+1} = \arg\max_{\delta\in\mathcal{I}_\delta} P(\hat{u}^{n+1},\delta)$ and set P^{n+1} as the corresponding maximum value;
3. $n = n+1$;

until $|P^n - P^{n-1}| > \varepsilon$;
$P_x = P^n$; $\hat{u}_x = \hat{u}^n$; $\hat{\delta}_x = \hat{\delta}^n$;
Initialization: $n = 0$
repeat (optimization for initial search direction given by δ)
1. Find $\hat{\delta}^{n+1} = \arg\max_{\delta\in\mathcal{I}_\delta} P(\hat{u}^n,\delta)$;
2. Find $\hat{u}^{n+1} = \arg\max_{u\in\mathcal{I}_u} P(u,\hat{\delta}^{n+1})$ and set P^{n+1} as the corresponding maximum value;
3. $n = n+1$;

until $|P^n - P^{n-1}| > \varepsilon$;
$P_y = P^n$; $\hat{u}_y = \hat{u}^n$; $\hat{\delta}_y = \hat{\delta}^n$;
if $P_x > P_y$ **then**
Output $\hat{u} = \hat{u}_x$ and $\hat{\delta} = \hat{\delta}_x$.
else
Output $\hat{u} = \hat{u}_y$ and $\hat{\delta} = \hat{\delta}_y$.
end

and

$$\delta_{\mathrm{CD}} = \hat{\delta}. \tag{17}$$

2) Adaptive Monopulse Procedure

The CD method is still time-consuming because of the 1-D searches involved during each iteration. To circumvent this drawback, in this subsection, the generalized monopulse approach is exploited [37] to approximate the optimal search in (12). To this end, let

$$\boldsymbol{h}_{\mathrm{AMP}} = \boldsymbol{h}_0 + \boldsymbol{C}(\boldsymbol{r} - \boldsymbol{\mu}), \tag{18}$$

where $\boldsymbol{h}_{\mathrm{AMP}} = [u_{\mathrm{AMP}},\delta_{\mathrm{AMP}}]^{\mathrm{T}} \in \mathbb{R}^2$ refers to the unknown parameters, $\boldsymbol{h}_0 = [u_0,\delta_0]^{\mathrm{T}} \in \mathbb{R}^2$, $\boldsymbol{C} = \begin{bmatrix} C_{xu} & C_{x\delta} \\ C_{yu} & C_{y\delta} \end{bmatrix} \in \mathbb{R}^{2\times 2}$ denotes a slope correction matrix, $\boldsymbol{\mu} = [\mu_x,\mu_y]^{\mathrm{T}} \in \mathbb{R}^2$ represents a bias correction vector, and $\boldsymbol{r} = [r_x,r_y]^{\mathrm{T}} \in \mathbb{R}^2$ refers to compressed measures, with r_x and r_y the monopulse ratios defined as

$$r_x = \Re\left\{\frac{\boldsymbol{d}_x^\dagger\boldsymbol{z}}{\boldsymbol{w}^\dagger\boldsymbol{z}}\right\}, \tag{19a}$$

$$r_y = \Re\left\{\frac{\boldsymbol{d}_y^\dagger\boldsymbol{z}}{\boldsymbol{w}^\dagger\boldsymbol{z}}\right\}. \tag{19b}$$

In (19a) and (19b) $\boldsymbol{w} = \boldsymbol{Q}^{-1}\boldsymbol{s}_0 \in \mathbb{C}^{MN}$ indicates the sum weight vector with $\boldsymbol{s}_0 = \boldsymbol{s}(u_0,\delta_0)$, $\boldsymbol{d}_x = \boldsymbol{Q}^{-1}\boldsymbol{s}_u \in \mathbb{C}^{MN}$ and $\boldsymbol{d}_y = \boldsymbol{Q}^{-1}\boldsymbol{s}_\delta \in \mathbb{C}^{MN}$ the difference beam weights, w.r.t. u and δ, respectively, where $\boldsymbol{s}_h = \frac{\partial\boldsymbol{s}}{\partial h}\big|_{(u_0,\delta_0)}, h \in \{u,\delta\}$. Detailed expressions for $\boldsymbol{s}_u$ and $\boldsymbol{s}_\delta$ are available in Appendix A.

The matrix $\boldsymbol{C}$ and the vector $\boldsymbol{\mu}$ are determined from the

vector-valued function $\boldsymbol{M}(u,\delta) \in \mathbb{R}^2$,

$$\boldsymbol{M}(u,\delta) = \boldsymbol{C}\left(\mathbb{E}\left[\boldsymbol{r}\right] - \boldsymbol{\mu}\right), \tag{20}$$

forcing the conditions

$$\boldsymbol{M}(u_0,\delta_0) = \boldsymbol{0}, \tag{21}$$

and

$$\boldsymbol{C}\ \mathbb{E}\left[\left(\frac{\partial \boldsymbol{r}}{\partial u}, \frac{\partial \boldsymbol{r}}{\partial \delta}\right)\right]\Big|_{(u_0,\delta_0)} = \boldsymbol{I}. \tag{22}$$

Under the Gaussianity assumption for the received data vector, the expectation of the monopulse ratios involved in (20), i.e., $\mathbb{E}\left[r_\alpha\right], \alpha \in \{x,y\}$, can be expressed as[1]

$$\begin{aligned}\mathbb{E}[r_\alpha] =& \mathbb{E}\left[\Re\left\{\frac{\boldsymbol{d}_\alpha^\dagger \boldsymbol{z}}{\boldsymbol{w}^\dagger \boldsymbol{z}}\right\}\right] = \\ =& \mathbb{E}\left[\Re\left\{\frac{\boldsymbol{d}_\alpha^\dagger \boldsymbol{z}\boldsymbol{z}^\dagger \boldsymbol{w}}{\boldsymbol{w}^\dagger \boldsymbol{z}\boldsymbol{z}^\dagger \boldsymbol{w}}\right\}\right] = \Re\left\{\frac{\boldsymbol{d}_\alpha^\dagger \mathbb{E}\left[\boldsymbol{z}\boldsymbol{z}^\dagger\right] \boldsymbol{w}}{\boldsymbol{w}^\dagger \mathbb{E}\left[\boldsymbol{z}\boldsymbol{z}^\dagger\right] \boldsymbol{w}}\right\} = \\ =& \frac{|\beta_1|^2 \Re\left\{\boldsymbol{d}_\alpha^\dagger \boldsymbol{s}\boldsymbol{s}^\dagger \boldsymbol{w}\right\} + \Re\left\{\boldsymbol{d}_\alpha^\dagger \boldsymbol{Q}\boldsymbol{w}\right\}}{|\beta_1|^2 \boldsymbol{w}^\dagger \boldsymbol{s}\boldsymbol{s}^\dagger \boldsymbol{w} + \boldsymbol{w}^\dagger \boldsymbol{Q}\boldsymbol{w}}, \quad \alpha \in \{x,y\},\end{aligned} \tag{23}$$

where $\boldsymbol{s} = \boldsymbol{s}\left(u,\delta\right)$. For a sufficiently high value of $|\beta_1|^2$, the two terms $\boldsymbol{d}_\alpha^\dagger \boldsymbol{Q}\boldsymbol{w}$ and $\boldsymbol{w}^\dagger \boldsymbol{Q}\boldsymbol{w}$, at the numerator and the denominator of (23), respectively, can be disregarded. As a result, the bias $\mathbb{E}[\boldsymbol{r}] = [\mathbb{E}[r_x],\ \mathbb{E}[r_y]]^{\mathrm{T}}$ correction values, fulfilling (21), can be approximated as

$$\mu_\alpha \ \approx\ \Re\left\{\frac{\boldsymbol{d}_\alpha^\dagger \boldsymbol{s}_0}{\boldsymbol{w}^\dagger \boldsymbol{s}_0}\right\}, \alpha \in \{x,y\}. \tag{24}$$

Besides, the slope correction matrix is computed according to (22), i.e.,

$$\begin{aligned}\boldsymbol{C} &= \left[\begin{array}{cc} C_{xu} & C_{x\delta} \\ C_{yu} & C_{y\delta} \end{array}\right] \\ &= \left[\begin{array}{cc} \mathbb{E}\left[\frac{\partial r_x}{\partial u}\right]\Big|_{(u_0,\delta_0)} & \mathbb{E}\left[\frac{\partial r_x}{\partial \delta}\right]\Big|_{(u_0,\delta_0)} \\ \mathbb{E}\left[\frac{\partial r_y}{\partial u}\right]\Big|_{(u_0,\delta_0)} & \mathbb{E}\left[\frac{\partial r_y}{\partial \delta}\right]\Big|_{(u_0,\delta_0)} \end{array}\right]^{-1},\end{aligned} \tag{25}$$

where $\mathbb{E}\left[\frac{\partial r_\alpha}{\partial h}\right]\Big|_{(u_0,\delta_0)}$, with $\alpha \in \{x,y\}, h \in \{u,\delta\}$, is approximated as (see [38, eq. 17])

$$\begin{aligned}&\mathbb{E}\left[\frac{\partial r_\alpha}{\partial h}\right]\Big|_{(u_0,\delta_0)} \approx \\ &\frac{\Re\left\{\boldsymbol{d}_\alpha^\dagger \boldsymbol{s}_h \boldsymbol{s}_0^\dagger \boldsymbol{w} + \boldsymbol{d}_\alpha^\dagger \boldsymbol{s}_0 \boldsymbol{s}_h^\dagger \boldsymbol{w}\right\}}{|\boldsymbol{w}^\dagger \boldsymbol{s}_0|^2} - \mu_\alpha 2\Re\left\{\frac{\boldsymbol{w}^\dagger \boldsymbol{s}_h}{\boldsymbol{w}^\dagger \boldsymbol{s}_0}\right\},\end{aligned} \tag{26}$$

Summarizing, the AMP procedure is synthetically reported in **Algorithm 2**. It is also worth pointing out that, as shown in [3], by further executing the procedure, namely, re-applying the monopulse algorithm employing the estimates $\hat{u}_{\mathrm{AMP}}$ and $\hat{\delta}_{\mathrm{AMP}}$ in place of the nominal u_0 and δ_0, the potential bias could be reduced, leading to some possible performance improvements. More in details, the, second iteration of **Algorithm 2** is performed using as input $\hat{u}_{\mathrm{AMP}}, \hat{\delta}_{\mathrm{AMP}}, \boldsymbol{Q}, \boldsymbol{s}_{\mathrm{AMP}}, \boldsymbol{s}_{\mathrm{AMP}-u}, \boldsymbol{s}_{\mathrm{AMP}-\delta}, \boldsymbol{z}$, where

[1]The "mean" is computed performing the expectation, w.r.t. the denominator, of conditional mean of the ratio given the denominator.

- $\boldsymbol{s}_{\mathrm{AMP}} = \boldsymbol{s}(\hat{u}_{\mathrm{AMP}}, \hat{\delta}_{\mathrm{AMP}})$ refers to the receive steering vector associated with the estimated direction and incremental range.
- $\boldsymbol{s}_{\mathrm{AMP}-u}$, and $\boldsymbol{s}_{\mathrm{AMP}-\delta}$ denote the partial derivatives of $s(u,\delta)$ w.r.t. u and δ, respectively computed at $(\hat{u}_{\mathrm{AMP}}, \hat{\delta}_{\mathrm{AMP}})$.

The overall procedure will be referred to as the double-step corrected (DSC) AMP (DSC-AMP) and could be also potentially iterated multiple times. The resulting estimates are denoted by $\hat{u}_{\text{DSC-AMP}}$ and $\hat{\delta}_{\text{DSC-AMP}}$, respectively.

Algorithm 2 FDA-AMP

Input: u_0, δ_0, $\boldsymbol{Q}$, $\boldsymbol{s}_0$, $\boldsymbol{s}_u$, $\boldsymbol{s}_\delta$, $\boldsymbol{z}$

Output: A solution $\hat{u}_{\mathrm{AMP}}$, $\hat{\delta}_{\mathrm{AMP}}$ to (11).

1. Compute $\boldsymbol{w} = \boldsymbol{Q}^{-1}\boldsymbol{s}_0$, $\boldsymbol{d}_x = \boldsymbol{Q}^{-1}\boldsymbol{s}_u$, and $\boldsymbol{d}_y = \boldsymbol{Q}^{-1}\boldsymbol{s}_\delta$;
2. Evaluate $r_\alpha = \Re\left\{\frac{\boldsymbol{d}_\alpha^\dagger \boldsymbol{z}}{\boldsymbol{w}^\dagger \boldsymbol{z}}\right\}, \alpha = x,y$ to obtain $\boldsymbol{r} = [r_x,\ r_y]^{\mathrm{T}}$;
3. Compute $\boldsymbol{\mu} = [\mu_x,\ \mu_y]^{\mathrm{T}}$ via (24) and $\boldsymbol{C}$ using (25);
4. Determine $\boldsymbol{h}_{\mathrm{AMP}}$ using (18);
5. Project the candidate solution $\boldsymbol{h}_{\mathrm{AMP}}$ onto $[-1,1] \times [-\frac{\Delta f}{B}, \frac{\Delta f}{B}]$ to get an estimate $\hat{\boldsymbol{h}}_{\mathrm{AMP}}$ complying with the problem constraints.

Output $[\hat{u}_{\mathrm{AMP}}, \hat{\delta}_{\mathrm{AMP}}]^{\mathrm{T}} = \hat{\boldsymbol{h}}_{\mathrm{AMP}}$.

3) Adaptive Generalized Monopulse Procedure with Complex Correction (AGMP-CC)

As the generalized monopulse approach procedure in (18) assumes real slope and bias correction, a more general procedure calls for a complex slope and bias correction [39]. This is the rationale followed in this section which is focused on the AGMP-CC, given by

$$\boldsymbol{h}_{\text{AGMP-CC}} = \boldsymbol{h}_0 + \Re\left\{\hat{\boldsymbol{C}}^\dagger(\hat{\boldsymbol{r}} - \hat{\boldsymbol{\mu}})\right\}, \tag{27}$$

where $\boldsymbol{h}_{\text{AGMP-CC}} = [u_{\text{AGMP-CC}}\ \delta_{\text{AGMP-CC}}]^{\mathrm{T}} \in \mathbb{R}^2$, $\boldsymbol{h}_0 = [u_0, \delta_0]^{\mathrm{T}} \in \mathbb{R}^2$ denotes the nominal values of the unknowns, $\hat{\boldsymbol{C}} \in \mathbb{C}^{2\times 2}$ denotes a complex slope correction matrix, $\hat{\boldsymbol{\mu}} \in \mathbb{C}^2$ indicates a bias correction vector, i.e., $\hat{\boldsymbol{\mu}} = [\tilde{\mu}_x,\ \tilde{\mu}_y]^{\mathrm{T}}$ with $\tilde{\mu}_\alpha = \frac{\boldsymbol{d}_\alpha^\dagger \boldsymbol{s}_0}{\boldsymbol{w}^\dagger \boldsymbol{s}_0}$, $\alpha \in \{x,y\}$ (obtained following the same line of reasoning as in [39]), and $\hat{\boldsymbol{r}} \in \mathbb{C}^2$ represents the complex monopulse ratio vector, i.e., $\hat{\boldsymbol{r}} = [\tilde{r}_x,\ \tilde{r}_y]^{\mathrm{T}}$ with

$$\tilde{r}_\alpha = \frac{\boldsymbol{d}_\alpha^\dagger \boldsymbol{z}}{\boldsymbol{w}^\dagger \boldsymbol{z}},\ \alpha \in \{x,y\}. \tag{28}$$

Now, substituting $\boldsymbol{z} = \beta_1 \boldsymbol{s} + \boldsymbol{n}$ into (28), and after some algebra and approximations as in [39], the following equation involving the actual unknowns, i.e., $\boldsymbol{h} = [u,\delta]^{\mathrm{T}}$, is obtained

$$(\tilde{\boldsymbol{r}} - \tilde{\boldsymbol{\mu}}) = \boldsymbol{B}_1(\boldsymbol{h} - \boldsymbol{h}_0) + \boldsymbol{p}_1, \tag{29}$$

where $\tilde{\boldsymbol{r}} \in \mathbb{C}^4$ represents the monopulse ratio vector whose entries are the complex monopulse ratios and their complex conjugates, i.e., $\tilde{\boldsymbol{r}} = [\hat{\boldsymbol{r}}^{\mathrm{T}}, \hat{\boldsymbol{r}}^{*\mathrm{T}}]^{\mathrm{T}}$,

- $\tilde{\boldsymbol{\mu}} = [\hat{\boldsymbol{\mu}}^{\mathrm{T}}, \hat{\boldsymbol{\mu}}^{*\mathrm{T}}]^{\mathrm{T}} \in \mathbb{C}^4$.
- $\boldsymbol{B}_1 = \left[\hat{\boldsymbol{B}}^{\mathrm{T}}, \hat{\boldsymbol{B}}^{*\mathrm{T}}\right]^{\mathrm{T}} \in \mathbb{C}^{4\times 2}$ where $\hat{\boldsymbol{B}} = \left[\begin{array}{cc} B_{xu} & B_{x\delta} \\ B_{yu} & B_{y\delta} \end{array}\right]$ with $B_{\alpha h} = \frac{\boldsymbol{d}_\alpha^\dagger \boldsymbol{s}_h \boldsymbol{w}^\dagger \boldsymbol{s}_0 - \boldsymbol{d}_\alpha^\dagger \boldsymbol{s}_0 \boldsymbol{w}^\dagger \boldsymbol{s}_h}{(\boldsymbol{w}^\dagger \boldsymbol{s}_0)^2}$ $(\alpha \in \{x,y\}, h \in$

$\{u, \delta\}$).

- $\boldsymbol{p}_1 = [\hat{\boldsymbol{p}}^{\mathrm{T}}, \hat{\boldsymbol{p}}^{*\mathrm{T}}]^{\mathrm{T}} \in \mathbb{C}^4$ where $\hat{\boldsymbol{p}} = [p_x,\ p_y]^{\mathrm{T}}$ with $p_\alpha = \frac{\boldsymbol{d}_\alpha^\dagger \tilde{\boldsymbol{p}}}{\beta_1 \boldsymbol{w}^\dagger \boldsymbol{s}},\ \alpha \in \{x, y\}$.
- $\tilde{\boldsymbol{p}} = \boldsymbol{n} - \left(\frac{\boldsymbol{w}^\dagger \boldsymbol{n}}{\boldsymbol{w}^\dagger \boldsymbol{s}}\right) \boldsymbol{s} \in \mathbb{C}^{MN}$.

Equation (29) poses an important constraint on the matrix $\hat{\boldsymbol{C}}$, so as to obtain in absence of noise and under the validity of (29) the exact values of the parameters via (27), i.e.,

$$\boldsymbol{C}_1^\dagger \boldsymbol{B}_1 = 2\boldsymbol{I}. \tag{30}$$

where $\boldsymbol{C}_1 = [\hat{\boldsymbol{C}}; \hat{\boldsymbol{C}}^*] \in \mathbb{C}^{4\times 2}$.

After some algebra, (30) can be recast as

$$\Re\left\{\hat{\boldsymbol{C}}^\dagger \hat{\boldsymbol{B}}\right\} = \boldsymbol{I}. \tag{31}$$

Hence, by substituting (31) and (29) into (27), it yields

$$\begin{aligned} \boldsymbol{h}_{\text{AGMP-CC}} - \boldsymbol{h}_0 = \Re\left\{\hat{\boldsymbol{C}}^\dagger(\hat{\boldsymbol{r}} - \hat{\boldsymbol{\mu}})\right\} = \\ = (\boldsymbol{h} - \boldsymbol{h}_0) + \Re\left\{\hat{\boldsymbol{C}}^\dagger \hat{\boldsymbol{p}}\right\}. \end{aligned} \tag{32}$$

It can be seen that the estimates $\boldsymbol{h}_{\text{AGMP-CC}}$ will be closest to the true value, i.e., $\boldsymbol{h}$, when the noise term effect, i.e., $\Re\left\{\hat{\boldsymbol{C}}^\dagger \hat{\boldsymbol{p}}\right\}$, is minimised. Following [39], the mean square value of the noise error terms on the u and δ components, is minimized according to

$$\begin{cases} \min\limits_{\hat{\boldsymbol{C}}_u} \quad \hat{\boldsymbol{C}}_u^\dagger \boldsymbol{Z}_1 \hat{\boldsymbol{C}}_u \quad \& \quad \min\limits_{\hat{\boldsymbol{C}}_\delta} \quad \hat{\boldsymbol{C}}_\delta^\dagger \boldsymbol{Z}_1 \hat{\boldsymbol{C}}_\delta \\ \text{s.t.} \quad \Re\left\{\hat{\boldsymbol{C}}^\dagger \hat{\boldsymbol{B}}\right\} = \boldsymbol{I}, \end{cases} \tag{33}$$

where $\hat{\boldsymbol{C}}_u \in \mathbb{C}^2$, $\hat{\boldsymbol{C}}_\delta \in \mathbb{C}^2$ denote the first and second columns of $\hat{\boldsymbol{C}}$ and the matrix $\boldsymbol{Z}_1 \in \mathbb{C}^{2\times 2}$ is constructed as [39]

$$\boldsymbol{Z}_1 = \boldsymbol{\Omega}^\dagger \boldsymbol{\Lambda} \boldsymbol{\Omega}, \tag{34}$$

where $\boldsymbol{\Omega} = [\boldsymbol{d}_x, \boldsymbol{d}_y] \in \mathbb{C}^{MN\times 2}$ and $\boldsymbol{\Lambda} = \mathbb{E}\left[\tilde{\boldsymbol{p}}_0 \tilde{\boldsymbol{p}}_0^\dagger\right] \in \mathbb{C}^{MN\times MN}$ with $\tilde{\boldsymbol{p}}_0 = \tilde{\boldsymbol{p}}|_{\boldsymbol{s}=\boldsymbol{s}_0} = \boldsymbol{n} - \left(\frac{\boldsymbol{w}^\dagger \boldsymbol{n}}{\boldsymbol{w}^\dagger \boldsymbol{s}_0}\right) \boldsymbol{s}_0$.

Standard optimization theory argumentation leads to the following expression for the optimal solution

$$\hat{\boldsymbol{C}}_{\text{opt}} = \boldsymbol{Z}_1^{-1} \hat{\boldsymbol{B}} \left(\Re\left\{\hat{\boldsymbol{B}}^\dagger \boldsymbol{Z}_1^{-1} \hat{\boldsymbol{B}}\right\}\right)^{-1}. \tag{35}$$

Finally, the estimates of u and δ can be obtained according to (27), i.e.,

$$\begin{aligned} \boldsymbol{h}_{\text{AGMP-CC}} = & \Re\left\{\left(\Re\left\{\hat{\boldsymbol{B}}^\dagger \boldsymbol{Z}_1^{-1} \hat{\boldsymbol{B}}\right\}\right)^{-1} \hat{\boldsymbol{B}}^\dagger \boldsymbol{Z}_1^{-1} (\hat{\boldsymbol{r}} - \hat{\boldsymbol{\mu}})\right\} \\ & + \boldsymbol{h}_0. \end{aligned} \tag{36}$$

The complete procedure for the AGMP-CC is provided in **Algorithm 3**.

Along the same line of reasoning followed to introduce the DSC-AMP estimator, a refined version of the AGMP-CC procedure can be conceived via a second execution of **Algorithm 3**, with inputs induced by $\hat{u}_{\text{AGMP-CC}}$ and $\hat{\delta}_{\text{AGMP-CC}}$. This procedure will be denoted as the DSC-AGMP-CC and $\hat{u}_{\text{DSC-AGMP-CC}}$ and $\hat{\delta}_{\text{DSC-AGMP-CC}}$ indicate the resulting estimates.

Algorithm 3 FDA-AGMP-CC

Input: u_0, δ_0, $\boldsymbol{Q}$, $\boldsymbol{s}_0$, $\boldsymbol{s}_u$, $\boldsymbol{s}_\delta$, $\boldsymbol{z}$

Output: A solution $\hat{u}_{\text{AGMP-CC}}$, $\hat{\delta}_{\text{AGMP-CC}}$ to (11) .

1. Compute $\boldsymbol{w} = \boldsymbol{Q}^{-1}\boldsymbol{s}_0$, $\boldsymbol{d}_x = \boldsymbol{Q}^{-1}\boldsymbol{s}_u$, and $\boldsymbol{d}_y = \boldsymbol{Q}^{-1}\boldsymbol{s}_\delta$;
2. Evaluate $\hat{\boldsymbol{r}} = [\tilde{r}_x,\ \tilde{r}_y]^{\mathrm{T}}$ with $\tilde{r}_\alpha$ given by (28);
3. Compute
   - $\hat{\boldsymbol{\mu}} = [\tilde{\mu}_x,\ \tilde{\mu}_y]^{\mathrm{T}}$ with $\tilde{\mu}_\alpha = \frac{\boldsymbol{d}_\alpha^\dagger \boldsymbol{s}_0}{\boldsymbol{w}^\dagger \boldsymbol{s}_0},\ \alpha \in \{x, y\}$.
   - $\hat{\boldsymbol{B}} = \begin{bmatrix} B_{xu} & B_{x\delta} \\ B_{yu} & B_{y\delta} \end{bmatrix}$, with $B_{\alpha h} = \frac{\boldsymbol{d}_\alpha^\dagger \boldsymbol{s}_h \boldsymbol{w}^\dagger \boldsymbol{s}_0 - \boldsymbol{d}_\alpha^\dagger \boldsymbol{s}_0 \boldsymbol{w}^\dagger \boldsymbol{s}_h}{(\boldsymbol{w}^\dagger \boldsymbol{s}_0)^2},\ \alpha \in \{x, y\}, h \in \{u, \delta\}$.
   - $\boldsymbol{Z}_1$ according to (34).
   - $\hat{\boldsymbol{C}}_{\text{opt}}$ using (35).
4. Evaluate $\boldsymbol{h}_{\text{AGMP-CC}}$ using (36);
5. Project $\boldsymbol{h}_{\text{AGMP-CC}}$ onto $[-1, 1] \times [-\frac{\Delta f}{B}, \frac{\Delta f}{B}]$ to get an estimate $\hat{\boldsymbol{h}}_{\text{AGMP-CC}}$ complying with the problem constraints. Output $[\hat{u}_{\text{AGMP-CC}}, \hat{\delta}_{\text{AGMP-CC}}]^{\mathrm{T}} = \hat{\boldsymbol{h}}_{\text{AGMP-CC}}$.

C. Discussion on the Computational Complexity

In this subsection, the assessment of the computational burden involved by the proposed estimators is provided[2]. To this end, the following equivalent expression of the objective function (12), that can be derived according to the results of Appendix B of [29], is used for ML and CD methods

$$P(u, \delta) = \frac{\left|\boldsymbol{a}(\delta)^\dagger\, \boldsymbol{v}(u)\right|}{\boldsymbol{a}(\delta)^\dagger\, \hat{\boldsymbol{T}}(u)\, \boldsymbol{a}(\delta)}, \tag{37}$$

where

$$\boldsymbol{v}(u) = \boldsymbol{c}(u) \odot \tilde{\boldsymbol{z}}(u) \in \mathbb{C}^M, \tag{38}$$

with

- $\tilde{\boldsymbol{z}}(u) = \sum_{l=1}^N [\boldsymbol{b}(u)]_l^* \bar{\boldsymbol{z}}_l \in \mathbb{C}^M$.
- $\bar{\boldsymbol{z}} = \boldsymbol{Q}^{-1}\boldsymbol{z} = [\bar{\boldsymbol{z}}_1^{\mathrm{T}}, \ldots, \bar{\boldsymbol{z}}_N^{\mathrm{T}}]^{\mathrm{T}} \in \mathbb{C}^{MN}$, $\bar{\boldsymbol{z}}_l \in \mathbb{C}^M$

and

$$\hat{\boldsymbol{T}}(u) = \boldsymbol{C}^\dagger(u)\, \boldsymbol{T}(u)\, \boldsymbol{C}(u) \in \mathbb{H}^M, \tag{39}$$

with

- $\boldsymbol{C}(u) = \mathrm{diag}(\boldsymbol{c}(u)) \in \mathbb{C}^{M\times M}$.
- $\boldsymbol{T}(u) = \sum_{k=1}^N \sum_{l=1}^N \left([\boldsymbol{b}(u)]_l^* \tilde{\boldsymbol{Q}}_{l,k} [\boldsymbol{b}(u)]_k\right)$.
- $\boldsymbol{Q}^{-1} = \begin{bmatrix} \tilde{\boldsymbol{Q}}_{1,1} & \cdots & \tilde{\boldsymbol{Q}}_{1,N} \\ \vdots & \ddots & \vdots \\ \tilde{\boldsymbol{Q}}_{N,1} & \cdots & \tilde{\boldsymbol{Q}}_{N,N} \end{bmatrix}$, where $\tilde{\boldsymbol{Q}}_{l,k} \in \mathbb{C}^{M\times M}$, $(l, k) \in \{1, \ldots, N\}^2$.

Therefore, given $\bar{\boldsymbol{z}}$ (which requires $\mathcal{O}((MN)^2)$ operations), for any given u (38) can be evaluated with a computational complexity $\mathcal{O}(MN)$. Indeed, $\mathcal{O}(M)$ operations are needed in the Hadamard product, while the evaluation of $\tilde{\boldsymbol{z}}(u)$ involves $\mathcal{O}(MN)$ operations. Besides, the computational complexity connected with (39) is $\mathcal{O}((MN)^2)$, where the main task is the evaluation of $\boldsymbol{T}(u)$, demanding $\mathcal{O}((MN)^2)$ operations.

[2]Without loss of generality, it is assumed that $\boldsymbol{Q}^{-1}$ is pre-computed off-line. If adaptive implementations of the proposed methods are considered, i.e., $\boldsymbol{Q}$ is estimated resorting to secondary data, the term $(MN)^2 K$ has to be added in the computational complexity expressions, where $K \geq MN$ is the size of the secondary data set.

ML estimator. Being the feasible set $\mathcal{I}$ given by the Cartesian product of $\mathcal{I}_u$ and $\mathcal{I}_\delta$, the 2-D search is tantamount to performing N_u 1-D search, each at a given value of u, with δ the optimization variable. Exploiting (37), for $\hat{\boldsymbol{T}}(u)$ and $\boldsymbol{v}(u)$ given, each 1-D search requires $\mathcal{O}(N_\delta M^2)$ operations. Hence, the overall computational complexity is $\mathcal{O}(N_u((NM)^2 + N_\delta M^2)$, where $(NM)^2$ amounts for the computation of $\hat{\boldsymbol{T}}(u)$ and $\boldsymbol{v}(u)$.

FDA-CD. At each iteration of the CD method, the 1-D searches w.r.t. u and δ require $\mathcal{O}(N_u M^2)$ and $\mathcal{O}(N_\delta M^2)$ operations, respectively, provided that $\hat{\boldsymbol{T}}(u)$ and $\boldsymbol{v}(u)$ are pre-computed for each $u \in \mathcal{I}_u$. This last task involves $\mathcal{O}(N_u(MN)^2)$ operations. To proceed further, let us denote by $N_{it,CD} = N_{it,CD,x} + N_{it,CD,y}$ the total number of iterations of the CD method, where $N_{it,CD,x}$ and $N_{it,CD,y}$ refer to the number of iterations required by the first and second cycle, respectively (the former with initial search direction given by u, the latter by δ). Hence, the implementation of FDA-CD requires $\mathcal{O}(N_u(MN)^2 + N_{it,CD}(N_u + N_\delta)M^2)$ operations, where the first term is due the computation of $\hat{\boldsymbol{T}}(u)$ and $\boldsymbol{v}(u)$ for any $u \in \mathcal{I}_u$.

FDA-AMP and FDA-AGMP-CC. The evaluation of the terms $\boldsymbol{w}$, $\boldsymbol{d}_x$, and $\boldsymbol{d}_y$ involved in step 1 of both FDA-AMP and FDA-AGMP-CC is the most demanding task and requires $\mathcal{O}((NM)^2)$ operations. Furthermore, as to FDA-AMP, $\mathcal{O}(NM)$ operations are connected with the computation of $\boldsymbol{r}$, $\boldsymbol{\mu}$, and $\boldsymbol{C}$, whereas $\mathcal{O}(1)$ operations are necessary to perform steps 4 and 5. On the other hand, with reference to FDA-AGMP-CC, $\mathcal{O}(NM)$ amounts for the computation of of $\hat{\boldsymbol{r}}$, $\hat{\boldsymbol{\mu}}$, and $\hat{\boldsymbol{B}}$, while $\mathcal{O}((NM)^2)$ operations are necessary to determine $\boldsymbol{Z}_1$. Besides, the evaluation of $\hat{\boldsymbol{C}}_{opt}$ as well as the execution of steps 4 and 5 need $\mathcal{O}(1)$ operations. This implies that the computational complexity for both FDA-AMP and FDA-AGMP-CC is $\mathcal{O}((NM)^2)$.

Summarizing, the computational complexity connected with the implementation (either non-adaptive or adaptive) of the devised estimators is reported in Table I. Before concluding this subsection, it is worth observing that the ML procedure is the most demanding. In fact, it exhibits a computational burden always higher than the monopulse-based procedures, and requires more operations than the CD method, as long as $N_u N_\delta > N_{it,CD}(N_u + N_\delta)$, which is a condition always met in our numerical experiments.

IV. CRBs for FDA-MIMO radar

To shed light on the statistical efficiency of proposed estimators, the CRBs for angle and incremental range are derived. Let us first define three auxiliary vectors, i.e., $\boldsymbol{\xi} = \boldsymbol{Q}^{-\frac{1}{2}}\boldsymbol{s} \in \mathbb{C}^{MN}$, $\boldsymbol{\xi}_u = \boldsymbol{Q}^{-\frac{1}{2}}\boldsymbol{s}_u \in \mathbb{C}^{MN}$, and $\boldsymbol{\xi}_\delta = \boldsymbol{Q}^{-\frac{1}{2}}\boldsymbol{s}_\delta \in \mathbb{C}^{MN}$. The CRBs for angle and incremental range are derived assuming unknown β_1.

In this respect, let us introduce the vector $\boldsymbol{\gamma} \in \mathbb{R}^4$ containing the real-valued unknown parameters, $u, \delta, \bar{\beta}_1 = \Re\{\beta_1\}, \tilde{\beta}_1 = \Im\{\beta_1\}$, i.e., $\boldsymbol{\gamma} = [u, \delta, \bar{\beta}_1, \tilde{\beta}_1]^{\mathrm{T}}$. Hence, the CRBs for the unknown parameters are given by the diagonal elements of $\boldsymbol{D}_{\boldsymbol{\gamma}} = \boldsymbol{F}^{-1} \in \mathbb{R}^{4\times 4}$, where the Fisher Information Matrix (FIM) $\boldsymbol{F} \in \mathbb{R}^{4\times 4}$ can be computed via the Slepian-Bangs formula [2, p. 927, eq. 8.34], which yields

$$\begin{aligned}\boldsymbol{F} &= 2\Re\left\{\left(\frac{\partial \beta_1 \boldsymbol{s}}{\partial \boldsymbol{\gamma}^{\mathrm{T}}}\right)^{\dagger}\boldsymbol{Q}^{-1}\left(\frac{\partial \beta_1 \boldsymbol{s}}{\partial \boldsymbol{\gamma}^{\mathrm{T}}}\right)\right\} \\ &= 2\Re\left\{[\beta_1\boldsymbol{s}_u, \beta_1\boldsymbol{s}_\delta, \boldsymbol{s}, j\boldsymbol{s}]^{\dagger}\left(\boldsymbol{Q}^{-\frac{1}{2}}\right)^{\dagger}\right. \\ &\quad \left.\left(\boldsymbol{Q}^{-\frac{1}{2}}\right)[\beta_1\boldsymbol{s}_u, \beta_1\boldsymbol{s}_\delta, \boldsymbol{s}, j\boldsymbol{s}]\right\} \\ &= 2\Re\left\{[\beta_1\boldsymbol{\xi}_u, \beta_1\boldsymbol{\xi}_\delta, \boldsymbol{\xi}, j\boldsymbol{\xi}]^{\dagger}[\beta_1\boldsymbol{\xi}_u, \beta_1\boldsymbol{\xi}_\delta, \boldsymbol{\xi}, j\boldsymbol{\xi}]\right\}.\end{aligned} \tag{40}$$

Hence, the FIM can be expressed in block form as

$$\boldsymbol{F} = 2\begin{bmatrix} \boldsymbol{F}_{11} & \boldsymbol{F}_{12} \\ \boldsymbol{F}_{21} & \boldsymbol{F}_{22} \end{bmatrix}, \tag{41}$$

where $\boldsymbol{F}_{11} \in \mathbb{R}^{2\times 2}$, $\boldsymbol{F}_{12} \in \mathbb{R}^{2\times 2}$, $\boldsymbol{F}_{21} \in \mathbb{R}^{2\times 2}$, and $\boldsymbol{F}_{22} \in \mathbb{R}^{2\times 2}$ are respectively given by

$$\boldsymbol{F}_{11} = \begin{bmatrix} |\beta_1|^2\|\boldsymbol{\xi}_u\|^2 & |\beta_1|^2\Re\left\{\boldsymbol{\xi}_u^{\dagger}\boldsymbol{\xi}_\delta\right\} \\ |\beta_1|^2\Re\left\{\boldsymbol{\xi}_u^{\dagger}\boldsymbol{\xi}_\delta\right\} & |\beta_1|^2\|\boldsymbol{\xi}_\delta\|^2 \end{bmatrix}, \tag{42a}$$

$$\boldsymbol{F}_{12} = \begin{bmatrix} \Re\left\{\boldsymbol{\xi}_u^{\dagger}\boldsymbol{\xi}\beta_1^*\right\} & -\Im\left\{\boldsymbol{\xi}_u^{\dagger}\boldsymbol{\xi}\beta_1^*\right\} \\ \Re\left\{\boldsymbol{\xi}_\delta^{\dagger}\boldsymbol{\xi}\beta_1^*\right\} & -\Im\left\{\boldsymbol{\xi}_\delta^{\dagger}\boldsymbol{\xi}\beta_1^*\right\} \end{bmatrix}, \tag{42b}$$

$$\boldsymbol{F}_{21} = \boldsymbol{F}_{12}{}^{\mathrm{T}} \tag{42c}$$

$$\boldsymbol{F}_{22} = \|\boldsymbol{\xi}\|^2\begin{bmatrix} 1 & 0 \\ 0 & 1 \end{bmatrix}. \tag{42d}$$

Then, $\boldsymbol{D}_{\boldsymbol{\gamma}}$ can be calculated as the inverse of $\boldsymbol{F}$, i.e.,

$$\boldsymbol{D}_{\boldsymbol{\gamma}} = \boldsymbol{F}^{-1} = \frac{1}{2}\begin{bmatrix} \boldsymbol{G}_1^{-1} & \boldsymbol{G}_2 \\ \boldsymbol{G}_3 & \boldsymbol{G}_4^{-1} \end{bmatrix}, \tag{43}$$

where $\boldsymbol{G}_1 = \boldsymbol{F}_{11} - \boldsymbol{F}_{12}\boldsymbol{F}_{22}^{-1}\boldsymbol{F}_{21} \in \mathbb{R}^{2\times 2}$. The expression of $\boldsymbol{G}_1$ is given in (44). Hence, the CRBs for u and δ (analytical details are reported in Appendix B) are given by

$$D_u = \frac{|\beta_1|^2}{2\det(\boldsymbol{G}_1)}\left(\|\boldsymbol{\xi}_\delta\|^2 - \frac{\left|\boldsymbol{\xi}_\delta^{\dagger}\boldsymbol{\xi}\right|^2}{\|\boldsymbol{\xi}\|^2}\right), \tag{45}$$

and

$$D_\delta = \frac{|\beta_1|^2}{2\det(\boldsymbol{G}_1)}\left(\|\boldsymbol{\xi}_u\|^2 - \frac{\left|\boldsymbol{\xi}_u^{\dagger}\boldsymbol{\xi}\right|^2}{\|\boldsymbol{\xi}\|^2}\right). \tag{46}$$

V. Performance Analysis

In this section, numerical examples are provided to assess the performance of the proposed methods to estimate the target incremental range and angle of arrival with reference to a FDA-MIMO radar sensing system. To this end, a transmit uniform linear array (ULA) with $M = 4$ elements and a receive ULA with $N = 10$ elements, both pointing toward the boresight direction (i.e., $u_0 = 0$), are considered. Moreover, orthogonal baseband signals are radiated, i.e., $\boldsymbol{R} = \boldsymbol{I}$, whereas the spacing among the antennas is set to $d = \lambda_0/2$.

Resorting to Monte Carlo technique, the performance of the proposed methods is evaluated for both range and angle estimations. As figure of merit, the RMSE is considered, which

This article has been accepted for publication in IEEE Transactions on Aerospace and Electronic Systems. This is the author's version which has not been fully edited and content may change prior to final publication. Citation information: DOI 10.1109/TAES.2021.3083591

	Computational Costs	
Methods	Non-adaptive implementation	Adaptive implementation
ML	$\mathcal{O}(N_u((NM)^2+N_\delta M^2))$	$\mathcal{O}(N_u((NM)^2+N_\delta M^2)+(NM)^2K)$
FDA-CD	$\mathcal{O}(N_u(MN)^2+N_{it,CD}(N_u+N_\delta)M^2)$	$\mathcal{O}(N_u(MN)^2+N_{it,CD}(N_u+N_\delta)M^2+(NM)^2K)$
FDA-AMP	$\mathcal{O}((NM)^2)$	$\mathcal{O}((NM)^2K)$
FDA-AGMP-CC	$\mathcal{O}((NM)^2)$	$\mathcal{O}((NM)^2K)$

TABLE I: Computational complexity of the considered estimators.

$$\boldsymbol{G}_1=\boldsymbol{F}_{11}-\boldsymbol{F}_{12}\boldsymbol{F}_{22}^{-1}\boldsymbol{F}_{21}=|\beta_1|^2\begin{bmatrix}\|\boldsymbol{\xi}_u\|^2-\frac{\left|\boldsymbol{\xi}_u^\dagger\boldsymbol{\xi}\right|^2}{\|\boldsymbol{\xi}\|^2} & \Re\left\{\boldsymbol{\xi}_u^\dagger\boldsymbol{\xi}_\delta\right\}-\frac{\Re\left\{\boldsymbol{\xi}_u^\dagger\boldsymbol{\xi}\boldsymbol{\xi}^\dagger\boldsymbol{\xi}_\delta\right\}}{\|\boldsymbol{\xi}\|^2}\\ \Re\left\{\boldsymbol{\xi}_u^\dagger\boldsymbol{\xi}_\delta\right\}-\frac{\Re\left\{\boldsymbol{\xi}_u^\dagger\boldsymbol{\xi}\boldsymbol{\xi}^\dagger\boldsymbol{\xi}_\delta\right\}}{\|\boldsymbol{\xi}\|^2} & \|\boldsymbol{\xi}_\delta\|^2-\frac{\left|\boldsymbol{\xi}_\delta^\dagger\boldsymbol{\xi}\right|^2}{\|\boldsymbol{\xi}\|^2}\end{bmatrix}. \tag{44}$$

TABLE II: Simulation Parameters of FDA-MIMO Radar

Parameter	**Symbol**	**Value**
transmit elements	M	4
receive elements	N	10
bandwidth	B	1 MHz
frequency increment	Δf	0.5 MHz
nominal target angle	u_0	0
nominal target incremental range	δ_0	0
possible angle of the target	u	$-\frac{0.891}{2(N+M)}, 0, \frac{0.891}{2(N+M)}$
possible incremental range of the target	δ	$-\frac{\Delta f}{2B}, -\frac{\Delta f}{4B}, 0, \frac{\Delta f}{4B}, \frac{\Delta f}{2B}$
angle of the coherent repeater 1	u_1	$5\,\frac{0.891}{(N+M)}$
incremental range of the coherent repeater 1	δ_1	$\frac{\Delta f}{3B}$
angle of the coherent repeater 2	u_2	$-6\,\frac{0.891}{(N+M)}$
incremental range of the coherent repeater 2	δ_2	$-\frac{\Delta f}{8B}$

is computed as

$$\widehat{\mathrm{RMSE}}_u=\sqrt{\frac{1}{\mathrm{M_C}}\sum_{i=1}^{\mathrm{M_C}}\|u-\hat{u}_i\|^2}, \tag{47}$$

and

$$\widehat{\mathrm{RMSE}}_\delta=\sqrt{\frac{1}{\mathrm{M_C}}\sum_{i=1}^{\mathrm{M_C}}\left\|\delta-\hat{\delta}_i\right\|^2}, \tag{48}$$

where $\mathrm{M_C}=500$ indicates the number of Monte Carlo independent trials, u and δ denote the actual DOA and incremental range of the target, whereas $\hat{u}_i$ and $\hat{\delta}_i$ are the estimates provided at the i-th trial by a given technique.

The performance of the CD, AMP, and AGMP-CC algorithms are evaluated for several values of SINR, defined according to [40], as

$$\mathrm{SINR}=|\beta_1|^2\boldsymbol{s}^\dagger(u_0,\delta_0)\boldsymbol{Q}^{-1}\boldsymbol{s}(u_0,\delta_0). \tag{49}$$

Besides, $B=1$ MHz and $\Delta f=0.5$ MHz are considered, with the nominal parameters values set as $u_0=0$ and $\delta_0=0$, respectively. Tapered version of AMP and AGMP-CC, referred to as AMP$_t$ and AGMP-CC$_t$, respectively, are considered too. In particular, Taylor and Bayliss tapers [37], both with sidelobe level $(\mathrm{SLL})=30$ dB and $\bar{n}=4$, are used for sum and difference beamforming, respectively, where $\bar{n}$ indicates the number of nearly constant-level sidelobes adjacent to the mainlobe. The DSC versions of AMP, AMP$_t$, and AGMP-CC$_t$ algorithms, respectively denoted as DSC-AMP, DSC-AMP$_t$, and DSC-AGMP-CC$_t$, are also included in the reported analysis. Besides, since AGMP-CC is equivalent to AMP when tapering is not applied [39], only the AMP and DSC-AMP curves are displayed in the figures, without loss of generality. Finally, the CRBs for both angle and incremental range estimation are used as performance benchmarks.

In the following subsections, two different interference scenarios are examined. In the former, the useful signal is buried in white Gaussian noise; in the latter, white Gaussian noise plus two coherent repeaters, is considered. The values of the parameters involved in the analyzed case studies are listed in Table II.

A. White Noise Interference Scenario

Within this subsection, the overall disturbance is assumed composed of white Gaussian interference only. Therefore, its covariance matrix is modeled as $\boldsymbol{Q}=\sigma_n^2\boldsymbol{I}_{MN}$, where σ_n^2 is the power level, assumed without loss of generality equal to 0 dB.

Fig. 3 illustrates the RMSE versus SINR for three case studies assuming different values of the true angles and incremental ranges of the target. In particular, Figs. 3 (a) and (d) consider $u=-0.891/(2(N+M)),\ \delta=-\Delta f/(4B)$, Figs. 3 (b) and (e) assume $u=0,\ \delta=\Delta f/(4B)$, while Figs. 3 (c) and (f) suppose $u=0.891/(2(N+M)),\ \delta=\Delta f/(2B)$. The RMSE analysis w.r.t. u is reported in Figs. 3 (a), (b), and (c), whereas that w.r.t. δ in Figs. 3 (d), (e), and (f).

This article has been accepted for publication in IEEE Transactions on Aerospace and Electronic Systems. This is the author's version which has not been fully edited and content may change prior to final publication. Citation information: DOI 10.1109/TAES.2021.3083591

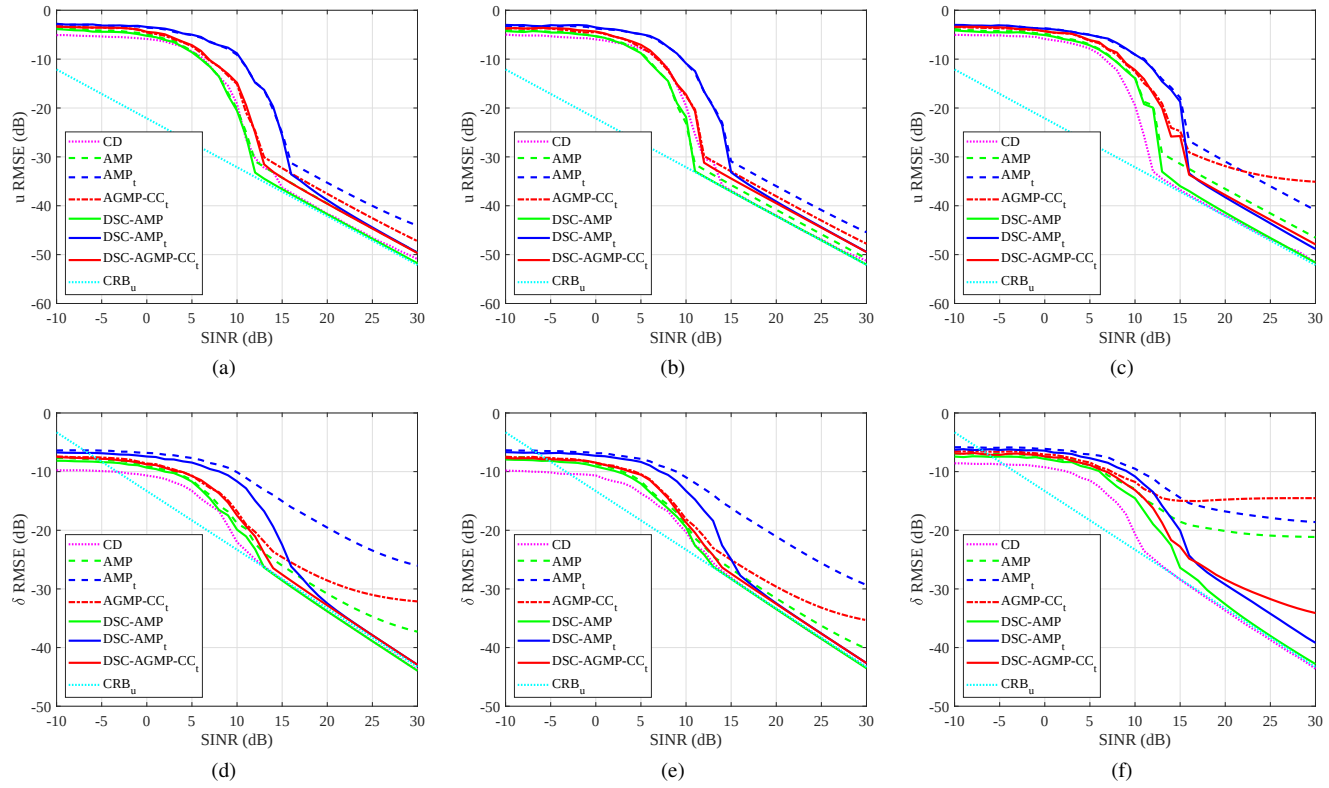

Fig. 3: Comparison of RMSE (dB) assuming white noise for some u and δ: (a) and (d) $u = -0.891/(2(N+M))$, $\delta = -\Delta f/(4B)$, (b) and (e) $u = 0$, $\delta = \Delta f/(4B)$, (c) and (f) $u = 0.891/(2(N+M))$, $\delta = \Delta f/(2B)$. The RMSE analysis w.r.t. u is reported in (a), (b), and (c), whereas that w.r.t. δ is reported in (d), (e), and (f).

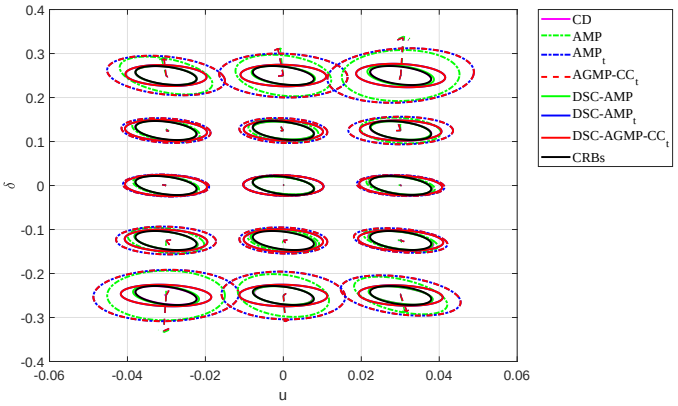

Fig. 4: Bias and variance analysis assuming white noise for 15 different pairs (u, δ) and SINR $= 20$dB.

Inspection of the curves shows that the higher the SINR the lower the RMSE of all the estimators. Besides, some of them achieve performance levels comparable with the CRB benchmark when the SINR is sufficiently high, for all the considered scenarios. Specifically, both the angle and incremental range estimates provided by the CD method are very close to their true values. Similar results hold for the DSC-AMP, with RMSE curves almost overlapped, especially for the high SINR regime, with those pertaining to CD technique. The plots also highlight that the DSC versions of the monopulse procedures outperform their corresponding single iteration (i.e., without DSC) counterparts for all the range of SINR values and all the considered experimental setups. Besides, the tapered procedures exhibit a performance degradation w.r.t. the unweighted counterparts. In particular, even with the further iteration, i.e., considering DSC-AMP$_t$ and DSC-AGMP-CC$_t$ at high SINR values, the CRB is not attained, in both u and δ domains. Furthermore, at low SINR, smaller RMSE values than the CRB benchmark are observed indicating that all the proposed estimators exhibit a bias under this SINR regime due to an upper bound to the mean square error induced by the enforced constraint.

To further shed light on performance of the different procedures, Fig. 4 displays the bias and variance ellipses of the proposed estimators for a grid of 15 points and SINR $= 20$dB. The ellipses corresponding to the CRBs are also reported for comparison. The simulation assumes the same interference environment as in Fig. 3. The results reveal that the AMP (or equivalently the AGMP-CC) method, as well as AMP$_t$ and AGMP-CC$_t$, exhibit a bias in both the u and δ domains, with a much more marked effect on the δ component. As expected, the bias is almost corrected by the second iteration of the double-step implementation, i.e., DSC-AMP and DSC-AGMP-CC, thus leading to a performance very close to the CRB. On the other hand, despite the second iteration, a small but noticeable bias persists in both DSC-AMP$_t$ and DSC-AGMP-CC$_t$. Therefore, the bias and variance analysis confirms that all the tapered monopulse algorithms experience a bias in both u and δ domains, which is the main reason for the deviations of these estimators from the CRB (at high

SINR). Finally, under this SINR regime, no bias is exhibited by the CD method with variance ellipses almost overlapped with CRBs.

B. Coherent Repeaters In The Interference Scenario

The interference scenario considered in this subsection accounts for the presence of two coherent signals at the same range ring as the target (this can be the situation of stand-off or escort jamming configuration), with signal-to-noise ratio (SNR) equal to 30 dB, impinging on the array from $u_1 = 5\ (0.891/(N+M))$ and $u_2 = -6\ (0.891/(N+M))$, with $\delta_1 = \Delta f/(3B)$ and $\delta_2 = -\Delta f/(8B)$, respectively. As a consequence, for this specific environment, the interference covariance matrix is modeled as $\boldsymbol{Q} = \sigma_n^2 \boldsymbol{I}_{MN} + \sigma_c^2 \boldsymbol{\Sigma}_c$ where σ_n^2 and σ_c^2 are the noise and interferers powers[3], respectively, with $\sigma_c^2/\sigma_n^2 = 30$ dB. Besides,

$$\boldsymbol{\Sigma}_c = \sum_{i=1}^{2} \boldsymbol{s}(u_i, \delta_i) \boldsymbol{s}^{\dagger}(u_i, \delta_i), \tag{50}$$

where $\boldsymbol{s}(u_i, \delta_i)$, u_i, and δ_i are the steering vector, the angle and the incremental range of the i-th coherent repeater, respectively.

The RMSE versus SINR is displayed in Fig. 5, where in each subfigure different values of the true angle and incremental range of the target are considered. In particular, Figs. 5 (a) and (d) refer to $u = 0.891/(2(N+M))$, $\delta = -\Delta f/(2B)$, Figs. 5 (b) and (e) assume $u = -0.891/(2(N+M))$, $\delta = -\Delta f/(4B)$, while Figs. 5 (c) and (f) consider $u = 0$, $\delta = 0$. The RMSE analysis w.r.t. u is reported in Figs. 5 (a), (b), and (c), whereas that w.r.t. δ in Figs. 5 (d), (e), and (f). Inspection of the curves highlights that the considered estimators exhibit performance behaviors comparable to those obtained in the white noise only scenario. In other words, the methods correctly estimate the parameters of a target located in the main beam without experiencing significant performance degradation due to possible coherent interferences. In particular, the CD and DSC-AMP procedures achieve similar RMSE levels with performance very close to CRB, at high SINR. Furthermore, the bias and variance analysis reported in Fig. 6, for SINR = 20dB, does not show specific differences w.r.t. the noise-only case, corroborating the effectiveness of the DSC technique to reduce the bias and thus improve the performance.

VI. Conclusion

The problem of target angle and incremental range estimation with a FDA-MIMO radar has been investigated using a single data snapshot. At the design stage, three estimators, with lower computational complexity than the 2-D grid search procedure required by the ML estimator, have been devised. Firstly, a CD algorithm has been proposed, which reduces the 2-D search to a sequence of 1-D problems alternating between the optimization over each variable while keeping the other fixed. Then, two approximated estimators, i.e., the

[3]The white noise power level σ_n^2 can be again assumed, without loss of generality, equal to 0 dB.

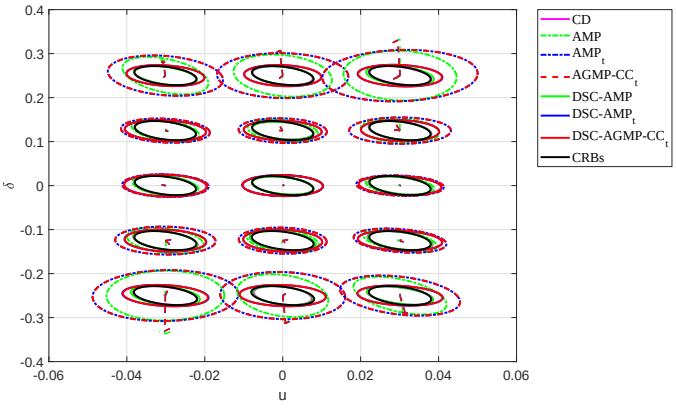

Fig. 6: Bias and variance analysis for 15 different pairs (u, δ) assuming SINR = 20dB and two coherent repeaters, with SNR = 30dB, located at $u_1 = 5\ (0.891/(N+M))$ and $u_2 = -6\ (0.891/(N+M))$ with incremental range of $\delta_1 = \Delta f/(3B)$ and $\delta_2 = -\Delta f/(8B)$, respectively.

AMP leveraging real slope and bias correction and the AGMP-CC capitalizing complex slope and bias correction, have been devised. The performance of the proposed estimators, also considering double-step and tapered versions, has been assessed in terms of RMSE versus SINR. Comparisons with benchmark limits, along with an extensive bias and variance analysis, have also been conducted. The results (for both white and colored interference) have pinpointed the effectiveness of the devised estimators to reliably estimate the angle and incremental range of the target in all the considered case studies. In particular, the CD method achieves a performance level very close to the theoretical CRBs when the SINR is sufficiently high.

Possible future research studies might include the design of estimators tailored for specific jammer and/or clutter scenarios, as well as the extension of the approach to the case of multiple targets via compressed sensing techniques. Furthermore, the analysis of the proposed estimators on real FDA-MIMO radar data represents definitely another research topic of primary concern.

Appendix

A. Expressions of the $\boldsymbol{s}_u$ and $\boldsymbol{s}_\delta$

According to (7), the first derivatives of $\boldsymbol{s}$ w.r.t. u and δ, evaluated respectively at u_0 and δ_0, can be calculated as

$$\begin{aligned} \boldsymbol{s}_u = \left.\frac{\partial \boldsymbol{s}}{\partial u}\right|_{(u_0,\delta_0)} &= \left.\frac{\partial \boldsymbol{b}(u)}{\partial u}\right|_{u_0} \otimes [\boldsymbol{c}(u_0) \odot \boldsymbol{a}(\delta_0)] \\ &+ \boldsymbol{b}(u_0) \otimes \left[\left.\frac{\partial \boldsymbol{c}(u)}{\partial u}\right|_{u_0} \odot \boldsymbol{a}(\delta_0)\right], \end{aligned} \tag{51}$$

and

$$\boldsymbol{s}_\delta = \left.\frac{\partial \boldsymbol{s}}{\partial \delta}\right|_{(u_0,\delta_0)} = \boldsymbol{b}(u_0) \otimes \left[\boldsymbol{c}(u_0) \odot \left.\frac{\partial \boldsymbol{a}(\delta)}{\partial \delta}\right|_{\delta_0}\right], \tag{52}$$

where

$$\left.\frac{\partial \boldsymbol{b}(u)}{\partial u}\right|_{u_0} = j2\pi \frac{d}{\lambda_0} \boldsymbol{E}_T \boldsymbol{b}(u_0), \tag{53}$$

This article has been accepted for publication in IEEE Transactions on Aerospace and Electronic Systems. This is the author's version which has not been fully edited and content may change prior to final publication. Citation information: DOI 10.1109/TAES.2021.3083591

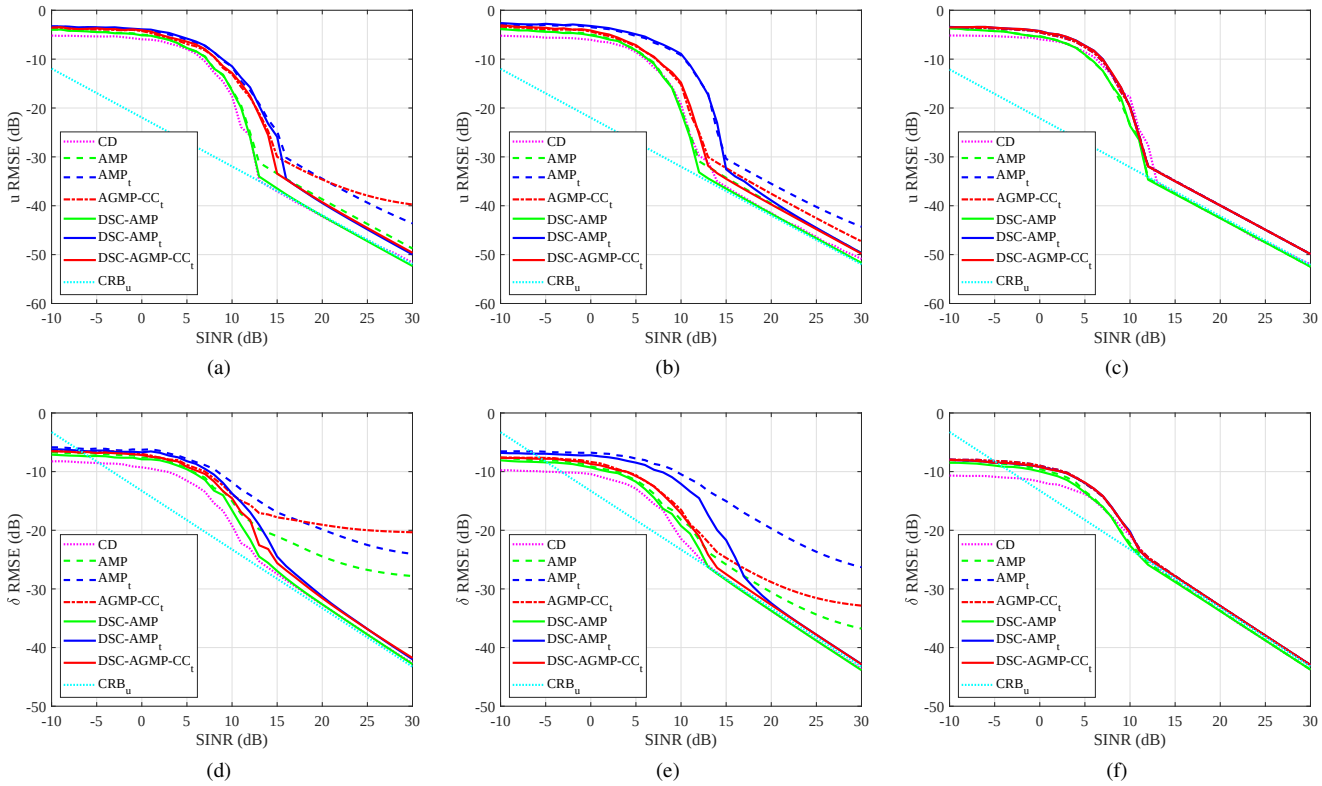

Fig. 5: Comparison of RMSE (dB) for some u and δ: (a) and (d) $u = 0.891/(2(N+M))$, $\delta = -\Delta f/(2B)$, (b) and (e) $u = -0.891/(2(N+M))$, $\delta = -\Delta f/(4B)$, (c) and (f) $u = 0$, $\delta = 0$, assuming two coherent repeaters, with SINR = 30dB, located at $u_1 = 5\,(0.891/(N+M))$ and $u_2 = -6\,(0.891/(N+M))$ with incremental range of $\delta_1 = \Delta f/(3B)$ and $\delta_2 = -\Delta f/(8B)$, respectively. The RMSE analysis w.r.t. u is reported in (a), (b), and (c), whereas that w.r.t. δ is reported in (d), (e), and (f).

$$\left.\frac{\partial \boldsymbol{c}\left(u\right)}{\partial u}\right|_{u_0} = \left.\frac{\partial\left(\boldsymbol{R}^{\mathrm{T}}\boldsymbol{d}(u)\right)}{\partial u}\right|_{u_0} = \boldsymbol{R}^{\mathrm{T}}\left.\frac{\partial \boldsymbol{d}\left(u\right)}{\partial u}\right|_{u_0} = j2\pi\frac{d}{\lambda_0}\boldsymbol{R}^{\mathrm{T}}\boldsymbol{E}_R\boldsymbol{d}(u_0), \tag{54}$$

$$\left.\frac{\partial \boldsymbol{a}\left(\delta\right)}{\partial \delta}\right|_{\delta_0} = j\pi\boldsymbol{E}_R\boldsymbol{a}\left(\delta_0\right), \tag{55}$$

with $\boldsymbol{E}_R = \mathrm{diag}\left([0,1,...,M-1]^{\mathrm{T}}\right)$ and $\boldsymbol{E}_T = \mathrm{diag}\left([0,1,...,N-1]^{\mathrm{T}}\right)$.

B. Computations of D_u and D_δ

Let us consider

$$\boldsymbol{V} = \boldsymbol{F}_{12}\boldsymbol{F}_{22}^{-1}\boldsymbol{F}_{21} = \|\boldsymbol{\xi}\|^{-2}\begin{bmatrix} V_{11} & V_{12} \\ V_{12} & V_{22}\end{bmatrix} \in \mathbb{R}^{2\times 2}, \tag{56}$$

The entries of $\boldsymbol{V}$ are given by

$$V_{11} = \Re^2\left\{\boldsymbol{\xi}_u^\dagger\boldsymbol{\xi}\beta_1^*\right\} + \Im^2\left\{\boldsymbol{\xi}_u^\dagger\boldsymbol{\xi}\beta_1^*\right\} = |\beta_1|^2\left|\boldsymbol{\xi}_u^\dagger\boldsymbol{\xi}\right|^2, \tag{57a}$$

$$\begin{aligned} V_{12} &= \Re\left\{\boldsymbol{\xi}_u^\dagger\boldsymbol{\xi}\beta_1^*\right\}\Re\left\{\boldsymbol{\xi}^\dagger\boldsymbol{\xi}_\delta\beta_1\right\} + \Im\left\{\boldsymbol{\xi}_u^\dagger\boldsymbol{\xi}\beta_1^*\right\}\Im\left\{\boldsymbol{\xi}^\dagger\boldsymbol{\xi}_\delta\beta_1\right\} \\ &= \Re\left\{\boldsymbol{\xi}_u^\dagger\boldsymbol{\xi}\beta_1^*\boldsymbol{\xi}^\dagger\boldsymbol{\xi}_\delta\beta_1\right\} = |\beta_1|^2\Re\left\{\boldsymbol{\xi}_u^\dagger\boldsymbol{\xi}\boldsymbol{\xi}^\dagger\boldsymbol{\xi}_\delta\right\}, \end{aligned} \tag{57b}$$

$$V_{22} = \Re^2\left\{\boldsymbol{\xi}_\delta^\dagger\boldsymbol{\xi}\beta_1^*\right\} + \Im^2\left\{\boldsymbol{\xi}_\delta^\dagger\boldsymbol{\xi}\beta_1^*\right\} = |\beta_1|^2\left|\boldsymbol{\xi}_\delta^\dagger\boldsymbol{\xi}\right|^2. \tag{57c}$$

Hence, $\boldsymbol{G}_1$ is derived as

$$\boldsymbol{G}_1 = \boldsymbol{F}_{11} - \boldsymbol{V} = \begin{bmatrix} G_{11} & G_{12} \\ G_{12} & G_{22}\end{bmatrix}, \tag{58}$$

with

$$G_{11} = |\beta_1|^2\|\boldsymbol{\xi}_u\|^2 - \frac{|\beta_1|^2}{\|\boldsymbol{\xi}\|^2}\left|\boldsymbol{\xi}_u^\dagger\boldsymbol{\xi}\right|^2, \tag{59}$$

$$G_{12} = |\beta_1|^2\Re\left\{\boldsymbol{\xi}_u^\dagger\boldsymbol{\xi}_\delta\right\} - \frac{|\beta_1|^2}{\|\boldsymbol{\xi}\|^2}\Re\left\{\boldsymbol{\xi}_u^\dagger\boldsymbol{\xi}\boldsymbol{\xi}^\dagger\boldsymbol{\xi}_\delta\right\}, \tag{60}$$

and

$$G_{22} = |\beta_1|^2\|\boldsymbol{\xi}_\delta\|^2 - \frac{|\beta_1|^2}{\|\boldsymbol{\xi}\|^2}\left|\boldsymbol{\xi}_\delta^\dagger\boldsymbol{\xi}\right|^2. \tag{61}$$

The inverse of $\boldsymbol{G}_1$ is given in (62), where $\det\left(\boldsymbol{G}_1\right) = G_{11}G_{22} - G_{12}G_{21}$. As a result, the CRBs for u and δ are the diagonal elements of $\frac{1}{2}\boldsymbol{G}_1^{-1}$, which have been provided in (45) and (46), respectively.

REFERENCES

[1] A. De Maio and M. Greco, Modern Radar Detection Theory. U.K.: The Institution of Engineering and Technology, 2015.

[2] H. L. Van Trees, Optimum array processing: Part IV of detection, estimation, and modulation theory, Wiley-Interscience, 2002.

[3] U. Nickel, "Monopulse estimation with adaptive arrays," *IEE Proc. F-Radar and Signal Process.*, vol. 140, no. 5, pp. 303-308, Oct. 1993.

[4] P. F. Kittredge and N. B. Pulsone, "Wideband angle estimation techniques for a beamspace application," in Proc. of the 2000 IEEE Sensor Array and Multi. Signal Process. Workshop (SAM 2000), Cambridge, MA, USA, 2000, pp. 474-478.

[5] L. Zhu, S. Qiu, and Y. Han, "Combined Constrained Adaptive Sum and Difference Beamforming in Monopulse Angle Esti-

$$\boldsymbol{G}_1^{-1} = \frac{1}{\det(\boldsymbol{G}_1)} \begin{bmatrix} G_{22} & -G_{12} \\ -G_{21} & G_{11} \end{bmatrix} = \frac{|\beta_1|^2}{\det(\boldsymbol{G}_1)} \begin{bmatrix} \|\boldsymbol{\xi}_\delta\|^2 - \frac{|\boldsymbol{\xi}_\delta^\dagger \boldsymbol{\xi}|^2}{\|\boldsymbol{\xi}\|^2} & -\Re\left\{\boldsymbol{\xi}_u^\dagger \boldsymbol{\xi}_\delta\right\} + \frac{\Re\left\{\boldsymbol{\xi}_u^\dagger \boldsymbol{\xi}\boldsymbol{\xi}^\dagger \boldsymbol{\xi}_\delta\right\}}{\|\boldsymbol{\xi}\|^2} \\ -\Re\left\{\boldsymbol{\xi}_u^\dagger \boldsymbol{\xi}_\delta\right\} + \frac{\Re\left\{\boldsymbol{\xi}_u^\dagger \boldsymbol{\xi}\boldsymbol{\xi}^\dagger \boldsymbol{\xi}_\delta\right\}}{\|\boldsymbol{\xi}\|^2} & \|\boldsymbol{\xi}_u\|^2 - \frac{|\boldsymbol{\xi}_u^\dagger \boldsymbol{\xi}|^2}{\|\boldsymbol{\xi}\|^2} \end{bmatrix}. \quad (62)$$

mation," *IEEE Antennas Wireless Propag. Lett.*, vol. 17, no. 12, pp. 2314-2318, Dec. 2018.

[6] S. Qiu, X. Ma, and W. Sheng, "A robust reduced-rank monopulse algorithm based on variable-loaded MWF with spatial blocking broadening and automatic rank selection," *Digital Signal Process.*, vol. 78, pp. 205-217, Jul. 2018.

[7] Y. Xu, X. Shi, W. Li, J. Xu, and L. Huang, "Low-sidelobe range-angle beamforming with FDA using multiple parameter optimization," *IEEE Trans. Antennas Propag.*, vol. 55, no. 5, pp. 2214-2225, Oct. 2019.

[8] Y. Ma, P. Wei, and H. Zhang, "General focusing beamformer for FDA: mathematical model and resolution analysis," *IEEE Trans. on Antennas Propag.*, vol. 67, no. 5, pp. 3089-3100, May 2019.

[9] B. Chen, X. Chen, Y. Huang, and G. Jian, "Transmit beampattern synthesis for the FDA radar," *IEEE Antennas Wireless Propag. Lett.*, vol. 17, no. 1, pp. 98-101, Jan. 2018.

[10] H. Shao, J. Dai, J. Xiong, H. Chen, and W. Wang, "Dot-shaped range-angle beampattern synthesis for frequency diverse array," *IEEE Antennas Wireless Propag. Lett.*, vol. 15, pp. 1703-1706, Feb. 2016.

[11] P. Antonik, M. C. Wicks, H. D. Griffiths, and C. J. Baker, "Frequency diverse array radars," *in Proc. of the IEEE Radar Conf.,* Verona, NY, USA, April 2006, pp. 215-217.

[12] W.-Q. Wang, "Overview of frequency diverse array in radar and navigation applications," *IET Radar, Sonar Navigat.*, vol. 10, no. 6, pp. 1001-1012, July 2016.

[13] A. Basit, W. Khan, S. Khan, and I. M. Qureshi, "Development of frequency diverse array radar technology: a review," *IET Radar, Sonar Navigat.*, vol. 12, no. 2, pp. 165-175, Feb. 2018.

[14] R. Gui, W.-Q. Wang, Y. Pan, and J. Xu, "Cognitive target tracking via angle-range-Doppler estimation with transmit subqperturing FDA radar," *IEEE J. of Sel. Topics in Signal Process.*, vol. 12, no. 1, pp. 76-89, Feb. 2018.

[15] C. Cui, J. Xiong, W. Wang and W. Wu, "Localization Performance Analysis of FDA Radar Receiver With Two-Stage Estimator," *IEEE Trans. Aerosp. Electron. Syst.*, vol. 54, no. 6, pp. 2873-2887, Dec. 2018.

[16] P. F. Sammartino, C. J. Baker, and H. D. Griffiths, "Frequency diverse MIMO techniques for radar," *IEEE Trans. Aerosp. Electron. Syst.*, vol. 49, no. 1, pp. 201-222, Jan. 2013.

[17] J. Xu, G. Liao, S. Zhu, and H. C. So, "Deceptive jamming suppression with frequency diverse MIMO radar," *Signal Process.*, vol. 113, pp. 9-17, Jan. 2015.

[18] J. Xu, G. Liao, Y. Zhang, H. Ji, and L. Huang, "An adaptive range-angle-Doppler processing approach for FDA-MIMO radar using three-dimensional localization," *IEEE J. of Sel. Topics in Signal Process.*, vol. 11, no. 2, pp. 309-320, Mar. 2017.

[19] C. Wang, J. Xu, G. Liao, X. Xu, and Y. Zhang, "A range ambiguity resolution approach for high-resolution and wide-swath SAR imaging using frequency diverse array," *IEEE J. of Sel. Topics in Signal Process.*, vol. 11, no. 2, pp. 336-346, Mar. 2017.

[20] B. Li, W. Bai, and G. Zheng, "Successive ESPRIT Algorithm for Joint DOA-Range-Polarization Estimation With Polarization Sensitive FDA-MIMO Radar," *IEEE Access*, vol. 6, pp. 36376-36382, June 2018.

[21] J. Xiong, W. Wang, and K. Gao, "FDA-MIMO Radar Range-Angle Estimation: CRLB, MSE, and Resolution Analysis," *IEEE Trans. Aerosp. Electron. Syst.*, vol. 54, no. 1, pp. 284-294, Feb. 2018.

[22] Y. Yan, J. Cai and W. Wang, "Two-stage ESPRIT for unambiguous angle and range estimation in FDA-MIMO radar," *Digit. Signal Process.*, vol. 92, pp. 151-165, Sep. 2019.

[23] W. Tang, H. Jiang and Q. Zhang, "Range-Angle Decoupling and Estimation for FDA-MIMO Radar via Atomic Norm Minimization and Accelerated Proximal Gradient," *IEEE Signal Process. Lett.,* vol. 27, pp. 366-370, Feb. 2020

[24] H. Chen and H. Shao, "Sparse reconstruction based target localization with frequency diverse array MIMO radar," 2015 IEEE China Summit and International Conference on Signal and Information Processing (ChinaSIP), Chengdu, 2015, pp. 94-98.

[25] C. Cui, J. Xu, R. Gui, W. Wang, and W. Wu, "Search-Free DOD, DOA and Range Estimation for Bistatic FDA-MIMO Radar," *IEEE Access*, vol. 6, pp. 15431-15445, Mar. 2018.

[26] K. Gao, W. Wang, and J. Cai, "Frequency diverse array and MIMO hybrid radar transmitter design via Cramr-Rao lower bound minimisation," *IET Radar, Sonar Naviga.,* vol. 10, no. 9, pp. 1660-1670, Dec. 2016.

[27] C. Wang, Z. Li, and X. Zhang, "FDA-MIMO for joint angle and range estimation: unfolded coprime framework and parameter estimation algorithm," *IET Radar, Sonar Navigation.,*, vol. 14, no. 6, pp. 917-926, June 2020.

[28] J. Xu, G. Liao, S. Zhu, L. Huang, and H. C. So, "Joint range and angle estimation using MIMO radar with frequency diverse array," *IEEE Trans. Signal Process.*, vol. 63, no. 13, pp. 3396-3410, July 2015.

[29] L. Lan, A. Marino, A. Aubry, A. De Maio, G. Liao, J. Xu, and Y. Zhang, "GLRT-Based Adaptive Target Detection in FDA-MIMO Radar," *IEEE Trans. Aerosp. Electron. Syst.*, vol. 57, no. 1, pp. 597-613, Feb. 2021.

[30] L. Lan, A. Marino, A. Aubry, A. De Maio, G. Liao, and J. Xu, "Design of adaptive detectors for FDA-MIMO radar", *IEEE 11th Sensor Array and Multichannel Signal Processing Workshop*, SAM 2020, 2020.

[31] L. Lan, A. Marino, A. Aubry, A. De Maio, G. Liao, and J. Xu, "Design of GLR-Based Detectors for FDA-MIMO radar," *IEEE 5th International Workshop on Metrology for AeroSpace*, MetroAeroSpace, 2020.

[32] R. C. Davis, L. E. Brennan, and L. S. Reed, "Angle Estimation with Adaptive Arrays in External Noise Fields," *IEEE Trans. Aerosp. Electron. Syst.*, vol. AES-12, no. 2, pp. 179-186, Mar. 1976.

[33] B. Chen, S. He, Z. Li, and S. Zhang, "Maximum Block Improvement and Polynomial Optimization," *SIAM J. on Optimization*, vol. 22, no. 1, pp. 87?07, Jan. 2012.

[34] M. Razaviyayn, M. Hong, and Z. Luo, "A Unified Convergence Analysis of Block Successive Minimization Methods for Nonsmooth Optimization," *SIAM J. on Optimization*, vol. 23, no. 2, pp. 1126-1153, 2013.

[35] A. Aubry, A. De Maio, A. Zappone, M. Razaviyayn, and Z. Luo, "A New Sequential Optimization Procedure and Its Applications to Resource Allocation for Wireless Systems," *IEEE Trans. Signal Process.*, vol. 66, no. 24, pp. 6518-6533, 15 Dec.15, 2018.

[36] P. Bertsekas, "Nonlinear programming," Athena Scientific, Belmont, Massachusetts, 1999.

[37] U. Nickel, "Overview of generalized monopulse estimation," *IEEE Trans. Aerosp. Electron. Syst. Mag.*, vol. 21, no. 6, pp. 27-56, June 2006.

[38] U. Nickel, "Monopulse estimation with subarray-adaptive arrays and arbitrary sum and difference beams," *IEE Proceedings - Radar, Sonar and Navigation*, vol. 143, no. 4, pp. 232-238, Aug. 1996.

[39] A. S. Paine, "Minimum variance monopulse technique for an adaptive phased array radar," *IEE Proc. Radar, Sonar and Naviga.*, vol. 145, no. 6, pp. 374-380, Dec. 1998.

[40] A. De Maio and D. Orlando, "Adaptive radar detection of a subspace signal embedded in subspace structured plus Gaussian interference via invariance," *IEEE Trans. Signal Process.*, vol. 64, no. 8, pp. 2156-2167, Apr. 2016.

Lan Lan (S'19-M'20) was born in Xi'an, China in 1993. She received her B.S. degree in Electronic Engineering, and the Ph.D. degree in signal and information processing, both from Xidian University, Xi'an, China, in 2015 and 2020, respectively. She has been a visiting Ph. D student in the University of Naples Federico II, Naples, Italy, from July 2019 to July 2020. She is currently a Tenure-track Associated Professor at the National Laboratory of Radar Signal Processing, Xidian University from August 2020. She was a recipient of the Excellent Paper Award at the CIE 2016 International Conference on Radar.

Her research interests include frequency diverse array radar systems, MIMO radar signal processing, target detection, and ECCM.

Massimo Rosamilia (S'20) received the B.S. (with honors) and M.S. degrees, both in computer engineering, from the University of Salerno, Italy, in 2017 and 2019, respectively. He is currently working towards the Ph.D. degree in information technologies and electrical engineering, University of Naples Federico II, Italy. His research interest lies in the field of statistical signal processing, with emphasis on radar signal processing. He ranked second in the Student Contest of the 1st International Virtual School on Radar Signal Processing, in 2020, with the contribution "Simultaneous Radar Detection and Constrained Target Angle Estimation via Dinkelbach Algorithm".

Augusto Aubry (M'12-SM'16) received the Dr. Eng. degree in telecommunication engineering (with honors) and the Ph.D. degree in electronic and telecommunication engineering both from the University of Naples Federico II, Naples, Italy, in 2007 and 2011, respectively. From February to April 2012, he was a Visiting Researcher with the Hong Kong Baptist University, Hong Kong. He is currently under research agreement with the Department of Electrical and Information Technology Engineering, University of Naples Federico II. His research interests include statistical signal processing and optimization theory, with emphasis on MIMO communications and radar signal processing. He is also the co-recipient of the 2013 Best Paper Award (entitled to B. Carlton) of the IEEE Transactions on Aerospace and Electronic Systems with the contribution Knowledge-Aided (Potentially Cognitive) Transmit Signal and Receive Filter Design in Signal-Dependent Clutter.

Antonio De Maio (S'01-A'02-M'03-SM'07-F'13) received the Dr. Eng. (Hons.) and Ph.D. degrees in information engineering from the University of Naples Federico II, Naples, Italy, in 1998 and 2002, respectively. From October to December 2004, he was a Visiting Researcher with the U.S. Air Force Research Laboratory, Rome, NY, USA. From November to December 2007, he was a Visiting Researcher with the Chinese University of Hong Kong, Hong Kong. He is currently a Professor with the University of Naples Federico II. His research interest lies in the field of statistical signal processing, with emphasis on radar detection, optimization theory applied to radar signal processing, and multiple-access communications. He is the recipient of the 2010 IEEE Fred Nathanson Memorial Award as the young (less than 40 years of age) AESS Radar Engineer 2010 whose performance is particularly noteworthy as evidenced by contributions to the radar art over a period of several years, with the following citation for "robust CFAR detection, knowledge-based radar signal processing, and waveform design and diversity". He is the corecipient of the 2013 best paper award (entitled to B. Carlton) of the IEEE TRANSACTIONS ON AEROSPACE AND ELECTRONIC SYSTEMS with the contribution "Knowledge-Aided (Potentially Cognitive) Transmit Signal and Receive Filter Design in Signal-Dependent Clutter".

Guisheng Liao (M'96-SM'16) was born in Guilin, Guangxi, China in 1963. He received his B.S. degree from Guangxi University, Guangxi, China, and M.S. and Ph.D. degrees from Xidian University, Xi'an, China, in 1985, 1990, and 1992, respectively.

He is currently a Yangtze River Scholars Distinguished Professor at the NationalLaboratory of Radar Signal Processing and serves asDean of the School of Electronic Engineering, in Xidian University. Since 2009, He has been the evaluation expert for the international cooperation project of Ministry of Science and Technology in China. Since 2007, he has been the lead of Yangtze River Scholars Innovative Team and devoted in advanced techniques in signal and information processing. Since 2006, he has served as the panelists for the medium and long term development plan in high-resolution and remote sensing systems. From 1999 to 2000, He has been a Senior Visiting Scholar in the Chinese University of Hong Kong, Hong Kong.

His research interests include array signal processing, space-time adaptive processing, radarwaveform design, and airborne/space surveillance andwarning radar systems.